DEVELOPMENT OF HARDWARE FOR IMPEDANCE CARDIOGRAPHY

A dissertation submitted in partial fulfillment of the requirements
for the degree of
Master of Technology
in Biomedical Engineering

by

N. S. Manigandan
(Roll No. 02330402)

under the supervision of

Prof. P. C. Pandey

Biomedical Engineering Group
School of Biosciences and Bioengineering
Indian Institute of Technology, Bombay
July 2004

ACKNOWLEDGEMENT

I would like to express my deepest gratitude to my guide Prof. P. C. Pandey for his guidance, support, and encouragement throughout the course of this project. I would like to thank Prof. Rakesh Lal for the suggestions he had given during my presentations.

I am thankful to Mr. Vinod Kumar Pandey for his help in recording and processing of signals. I would also like to thank Mr. Dinesh Choudhary for his suggestions and help with PCB layouts for this project. I would also like to thank Mr. Vidyadhar Kamble for his help in fabricating the PCB. I also thank all my friends in my lab for their help in taking the recordings.

N. S. Manigandan

July 2004

N. S. Manigandan / Prof. P. C. Pandey (supervisor): "Development of hardware for impedance cardiography", *M.Tech. dissertation*, Biomedical Engineering Group, School of Biosciences and Bioengineering, Indian Institute of Technology, Bombay, July 2004.

ABSTRACT

Impedance cardiography is a non-invasive technique for measuring cardiac output and for diagnosing cardiac disorders. The basal impedance of human thorax is normally 20 – 30 Ω and it decreases by 0.1 – 0.2 Ω. During systole, blood pumped into the thoracic region decreases the impedance. This change in the thoracic impedance is sensed by injecting a high frequency (20 – 100 kHz) current (< 5 mA) into the thoracic region through a pair of electrodes and by measuring the voltage across another pair of electrodes. The impedance variation thus measured is known as impedance cardiogram (ICG) and can be used for estimating stroke volume by using appropriate models of blood flow and can also be used for diagnostic information. This project involved developing an instrument to acquire the impedance cardiogram. The various signals that can be acquired from the instrument are basal impedance, impedance variation signal, and its derivative, and differentiated ECG (sensed from the same electrodes). Also a thoracic impedance simulator was developed for comprehensive testing and calibration of the impedance cardiograph instrument to ensure proper signal pick-up and detection of impedance variation.

CONTENTS

LIST OF SYMBOLS

Symbol	Explanation
ΔV	Volume change of the small parallel column
ρ	Resistivity of the material in the small parallel column
L	Length of the column
Z_o	Impedance of the fixed conduction volume
ΔZ	Impedance change across the column
$-(dz/dt)_{\max}$	Most negative (upward in the graph) deflection during systole measured from zero.
T_{lvet}	Left ventricle ejection time
Z_n	Impedance of changing volume
$z(t)$	Impedance signal
dz/dt	Differentiated impedance signal, impedance cardiogram (ICG)

LIST OF ABBREVIATIONS

Symbol	Explanation
ICG	Impedance cardiogram
ECG	Electrocardiogram
PCG	Phono cardiogram
CO	Cardiac output
SV	Stroke volume
ADC	Analog-to-digital converter
DAC	Digital-to-analog converter
PWM	Pulse width modulation
DC	Direct current
SAR	Successive approximation register
SNR	Signal-to-noise ratio
PCB	Printed circuit board
CM	Common mode
DM	Differential mode
CMRR	Common mode rejection ratio
BP	Blood pressure

LIST OF FIGURES

LIST OF TABLES

Chapter 1
INTRODUCTION

1.1 Background

Impedance cardiography is a non-invasive technique for measuring cardiac output and for diagnosing cardiac disorders. In heart during systole, blood pumped into the thoracic region changes its basal impedance. The basal impedance of thorax is normally in the range of 20 – 30 Ω, and this decreases by 0.1 – 0.2 Ω when the blood flows into the thorax [1] – [3]. This change in basal impedance is sensed by injecting a high frequency (20 – 100 kHz) current (1 – 5 mA) into the thoracic region through a pair of electrodes and by measuring the voltage across another pair of electrodes [3] – [6]. The impedance variation thus measured is known as impedance cardiogram (ICG) and can be used for estimating stroke volume (SV) by using appropriate models of blood flow and can also be used for diagnostic information [3] – [20].

1.2 Project objective

This project involved developing an instrument to acquire the impedance cardiogram. It is a continuation of earlier work done at IIT Bombay and involves modification and redesign of hardware for better performance [21] – [23]. The impedance cardiograph incorporates: (i) current injection section, (ii) impedance detection section, (iii) drift cancellation section, and (iv) ECG detection section. The current injection section has an oscillator and voltage to current converter. There are two types of voltage to current converter provided: unbalanced current source and balanced current source. To make optimal use of the ADC range, during signal acquisition, an automatic drift cancellation circuit has been developed. The ECG which is simultaneously acquired with ICG is used as a fiducial mark for ensemble averaging of the ICG signal, which is processed for obtaining the cardiac output and diagnostic information.

Also a thoracic impedance simulator was developed based on an earlier design, for comprehensive testing and calibration of the impedance cardiograph to ensure proper signal pick-up and detection of impedance variation. It provides the option of selecting one of the three different basal impedances provided for effective calibration of the impedance cardiograph. The percentage variation in the basal impedance can be varied over 1 – 2 %.

1.3 Dissertation outline

The second chapter gives the fundamentals of impedance cardiography. The third and fourth chapters give the hardware design of impedance cardiograph and thoracic simulator respectively. Test results for validation of the hardware developed are given in Chapter 5. In sixth chapter, the impedance cardiography results and possible improvements in hardware are discussed. The last chapter gives a summary of the work and some suggestion for future work.

Chapter 2
BASICS OF IMPEDANCE CARDIOGRAPHY

2.1 Introduction

Cardiac stroke volume (SV) is the amount of blood pumped during systole. Cardiac output (CO) is the amount of blood pumped by heart in one minute, and hence is given as the product of SV and heart beat rate [24]. In conventional methods Fick's dye dilution and thermo dye dilution methods are used to calculate the SV. Both the techniques above are invasive [1][24].

Impedance cardiography is a non-invasive technique to estimate cardiac output. Heart is situated in the thoracic region which is made of biological materials like bones and muscles. These biological materials are poor conductors of electricity and contributes a fixed impedance for thorax when compared to blood [5][9]. This characteristic of blood is used as the base for impedance cardiography. Heart during systole pumps blood into the pulmonary circulatory system and systemic circulatory system. The pulmonary circulation is concentrated over the thoracic region for purification of blood at lungs and the systemic circulation supplies pure blood to various parts of the body from heart through the aortic artery. Due to the flow of blood into the thoracic region through these two circulatory systems, the impedance of the thorax decreases. This impedance change in the thorax is a function of amount of blood pumped by the ventricles of the heart. The signal obtained corresponding to this impedance variation is known as impedance cardiogram. By sensing this signal, the SV can be estimated and used for calculating CO.

2.2 The impedance cardiography technique

Direct measurement of impedance across body tissues is difficult due to the capacitance between the sensing electrode and skin. To overcome this problem, high frequency current is injected into the thoracic region by a pair of injecting electrodes I1

and I2 and amplitude modulated voltage due to the change in impedance is picked up by the sensing electrodes E1 and E2. The basic block diagram is shown in Fig 2.1. The frequency of the injected current is kept typically between 20 – 100 kHz and the current between 1 – 5 mA. In this frequency range, the current path becomes nearly resistive and the effect of capacitance due to the cell walls become negligible. Also the effect of capacitance between the electrode and the skin is minimized [2][5]. If the injected current frequency is decreased below 20 kHz, there may be some biological effects. If the frequency is increased above 100 kHz then the current path does not include the deeper region of the thorax and hence the impedance variation is not sensed properly [1].

2.3 The heart

The anatomy of heart is shown in Fig 2.2. Human heart can be characterized as four separate chambers namely: the two atria and the two ventricles. The right atrium and ventricle is separated by the tricuspid valve. The left atrium and ventricle is separated by the mitral valve. The atrium pumps blood into ventricles which then pumps the blood into pulmonary and systemic circulation with large force. The basic pulmonary and systemic circulatory system is shown in Fig 2.3. The pulmonary circulatory system takes blood to the lungs for oxygenation and then back to heart. The systemic circulation takes oxygenated blood to various parts of the body. This process of pumping is called systole. During initial period of systole, pressure inside the ventricle increases with constant blood volume. When the intra-ventricular pressure exceeds the outside pressure, the aortic and pulmonary valves are opened and blood pours rapidly out of ventricles. This is called rapid ejection which takes place for one-third of the total ejection period. It is followed by slow ejection at the end of which the ventricular relaxation occurs causing the filling of ventricles again. Then a new cardiac cycle begins. This systolic action is carried out by action potentials generated by special type of heart pacemaker cells that constitute the sino-atrial (SA) node, and the atrio-ventricular (AV) node. This action potential is generated and transmitted in a rhythmic fashion, so as to maintain the rhythmicity of heart. The depolarizing phase of the action potential activates the contraction (systole) of the heart.

The left ventricular pressure which pumps blood to the various organs of the body is typically 120 – 130 mm Hg. The right ventricular pressure which pumps blood to the

thoracic region (pulmonary circulation) for oxygenation is 60 – 80 mm Hg. The left atrial pressure is 7 – 8 mm Hg and the right atrial pressure is 4 – 6 mm Hg. The stroke volume which is the amount of blood pumped into the aorta during one systole is about 70 ml and the cardiac output which is the amount of blood pumped by the heart in one minute is around 5 liters [24].

The activity of heart gives rise to a changing electrical dipole vector, which results in surface potentials. These picked up by means of limb and chest electrodes are known as the electrocardiogram (ECG). The flow of blood from the atrium and the ventricles are regulated by valves. These valves in their course of opening and closing produce vibrations which are referred to as heart sounds. These sounds picked up at the surface of the body are known as phonocardiogram (PCG). These ECG and PCG signals are used for diagnosis of various cardiac disorders. Various pressure and volumetric variation during the cardiac cycle are shown in Fig 2.4. The figure also shows ECG and PCG waveforms [24][25].

The SV which is the amount of blood pumped by the ventricles to the pulmonary and systemic circulatory system is regulated by the pulmonary and aortic valves respectively. Any disorder in heart valves like stenosis may lead to decreased stroke volume. The cause for decreased stroke volume may also be due to blockage in arteries and disorder in pacemaker cells.

2.4 Basic impedance model of thorax

Kubicek [12] proposed a parallel column model (Fig 2.5) to quantify the impedance change in thorax. This model depicts the lungs whose volume changes with the inflow of blood, which is the conducting medium. The model consists of a conducting material "M" with impedance Z_o, which is paralleled by a column "N" with uniform cross sectional area of length L and resistivity ρ. The conducting medium "M" depicts the bones and muscles of thorax which constitutes a constant impedance and the parallel column "N"; the blood which flows into the thoracic region and thus changing the net impedance of the thorax. It is to be noted that all the impedances in the model are purely resistive.

The net impedance of parallel column model is given by

$$Z(t) = Z_o \parallel Z_n \tag{2.1}$$

If the cross sectional area of the column "N" varies from zero to a finite value the change in impedance across the parallel column is given by

$$z(t) = Z(t) - Z_o$$

$$= -\frac{{Z_o}^2}{(Z_o + Z_n)} \tag{2.2}$$

Since $z(t) << Z_o$ we can assume $Z_n >> Z_o$ and we get

$$z(t) = -\frac{{Z_o}^2}{Z_n} \tag{2.3}$$

The impedance of the column N, with cross sectional area A, length L, and volume $\upsilon = LA$, is

$$Z_n = \frac{\rho L^2}{\upsilon} \tag{2.4}$$

Hence the impedance variation can be given as

$$z(t) = -\frac{{Z_o}^2 \upsilon}{\rho L^2} \tag{2.5}$$

Initially an assumption was made by Kubicek that inflow of blood into the lungs is the source of impedance change and the volume of the column N is zero before systole. So as blood flows into the lungs during systole the impedance starts decreasing and assuming no blood leaves the lungs during systole, the maximum impedance change can be written as

$$\Delta Z = (-z)_{\max}$$

Then the change in volume of the column can be written as

$$\Delta V = \rho \frac{L^2}{{Z_o}^2} \Delta Z \tag{2.6}$$

where

ΔV = the volume change of the small parallel column

ρ = the resistivity of the material in the small parallel column

L = the length of the column

Z_o = the impedance of the fixed conduction volume

ΔZ = the impedance change across the column

Here the outflow of blood from the lungs into the heart was not accounted during systole. Later a correction was made by Kinnen and Kubicek and reported by Malvino and Plonsey [26], in which the forward extrapolation technique shown in Fig 2.6, was introduced which also accounted for the outflow of blood from lungs into the heart during later part of systole. This resulted in modified Kubicek's formula as given below

$$\Delta V = \frac{\rho L^2}{Z_o^2}\left(-\frac{dz}{dt}\right)_{\max} T_{lvet} \qquad (2.7)$$

where

$-\frac{dz}{dt}_{\max}$ = the most negative (upward in the graph) deflection during systole measured from zero.

T_{lvet} = left ventricle ejection time (time between the first heart sound "B" and aortic valve closure "X") as shown in Fig 2.4.

This gives the stroke volume (ΔV) of the heart. The resistivity of the blood is of the order of 150 Ω-cm and the cardiac output is given by the product of heart rate and stroke volume.

2.5 Various parameters that influence impedance cardiography

2.5.1 Electrode placements and configuration

The placement of electrode to pick-up ICG signal plays a major role in impedance cardiography. The band-electrode configuration uses four band electrodes encircling the thorax, with the outer pair of electrodes delivering the high frequency current and the inner pair measuring the voltage. The measured base impedance of approximately 22 Ω typically changes by 0.25 Ω over a cardiac cycle. The advent of spot electrodes, introduced to improve the ease of electrode placement and comfort level for patients, opened up new possibilities for ICG.

In some improvements, spot electrodes are used for both current delivery and voltage pick-up, while in others spot electrodes are used only for voltage pick-up and band electrodes for current delivery. It was found that spot electrodes provide a better signal-to-noise ratio (SNR) than the band electrodes. This is because ICG signal varies

with electrode location, and spot electrodes can be placed where motion artifact is minimum, so it is possible to optimize spot-electrode location for best SNR during exercise, while band electrodes are limited in the choice of locations.

The baseline impedance measured with spot electrodes positioned laterally was significantly higher than that measured with band electrodes at the same level, causing the measured SV to be smaller than that measured with band electrodes. Also by moving the neck electrodes towards the top of the neck, the current-density field becomes more uniform and the ICG-based SV measurement appears more accurate [6][27].

Further there are two types of electrode configuration, 2-electrode and 4-electrode configuration. In the 2-electrode configuration the current is injected through the same electrodes which picks up the modulated voltage signal. The problem with the 2-electrode configuration was the current distribution and the electrode-skin contact impedance. In 4-electrode, the effect of skin-electrode contact impedance on voltage pick-up is minimized and the current distribution is better [28].

2.5.2 The effect of pulsative flow of blood

The resistivity of the blood changes during pulsative flow of blood due to the alignment of the erythrocytes. The peak resistivity change occurs at the same time as the peak in the impedance signal. So for exact calculation of the stroke volume this has to be taken into consideration [2][29].

2.5.3 Respiration

During respiration, the negative pressure inside the lungs not only increases the inflow of air into it but also increases the venous return. This may introduce an unwanted signal artifact which has to be eliminated [29].

2.5.4 Motion artifact

The main source of motion artifact in impedance signal is change in dimension of thorax while breathing. This will introduce a broad spectrum of amplitude and frequencies. And more over the frequency of motion artifact may fall well with in the signal frequency [29].

2.6 The impedance cardiogram

The impedance cardiogram simultaneously acquired with the ECG and PCG signals are shown in Fig 2.6. The basic impedance signal is the $z(t)$ waveform and the other one is the differentiated *dz/dt* of the above impedance signal which is the impedance cardiogram (ICG). The "R" point of ECG signal is used as the fiducial mark for ensemble averaging of the ICG signal and to get the left ventricle ejection time for calculating the cardiac output. The *dz/dt* signal is also used to get the $-(dz/dt)_{max}$. From $z(t)$ waveform, through extrapolation technique, ΔZ is calculated. The point "A" indicates the atrial activity of heart, "B" is synchronous with the first heart sound, "C" indicates the largest decrease in impedance during systole, "X" the aortic valve closure, "Y" pulmonary valve closure and "O" indicates the largest decrease in impedance during diastole and close in time to mitral valve opening [3].

2.7 Historical account of impedance cardiograph

The idea of impedance cardiography came from impedance plethysmography which is a technique to measure the electrical impedance in human body. Impedance plethysmography was introduced by Jan Nyboer in 1940. Later Kubicek extended this to measure the impedance change in thorax due to flow of blood from heart into the thorax. A dedicated instrument for impedance cardiography was reported by Zhang et al [6] in 1986.

Work on impedance cardiography has been carried out at IIT Bombay from 1990 onwards. An instrument for measuring the cardiac output and stroke volume was developed by Joshi in 1993 [22]. In 1997, Patwarthan developed a software for off-line display of all the recorded physiological signals and also developed a thoracic simulator for calibration of impedance cardiograph [23]. Later Kuriakose in 2000 modified the circuit to improve the sensitivity and consistency of the instrument [21].

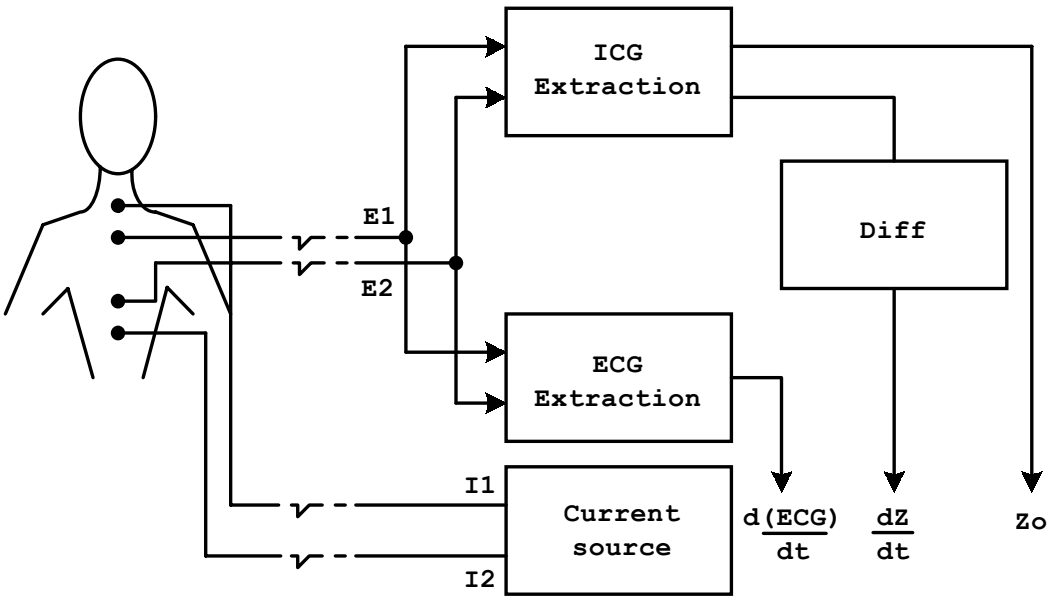

Fig 2.1 Block diagram of impedance cardiography [6]

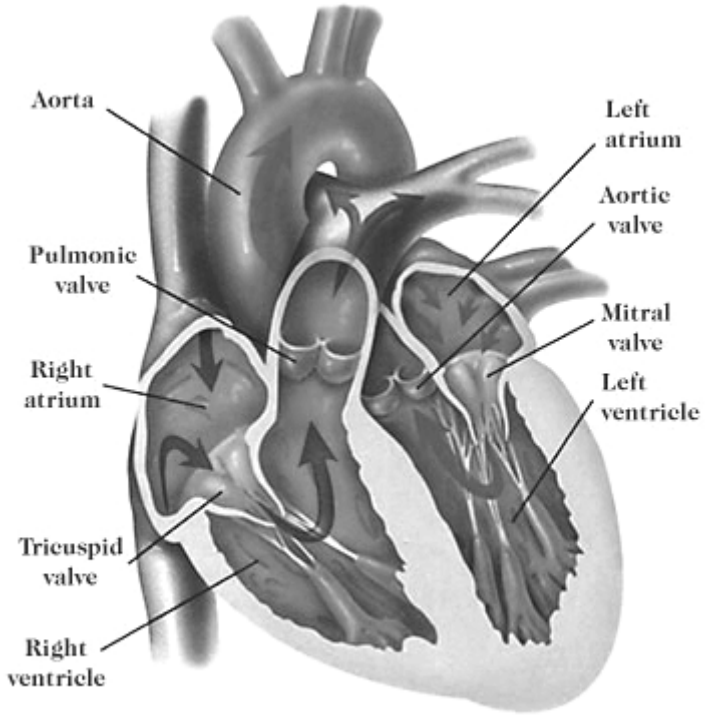

Fig 2.2 Anatomy of heart [34]

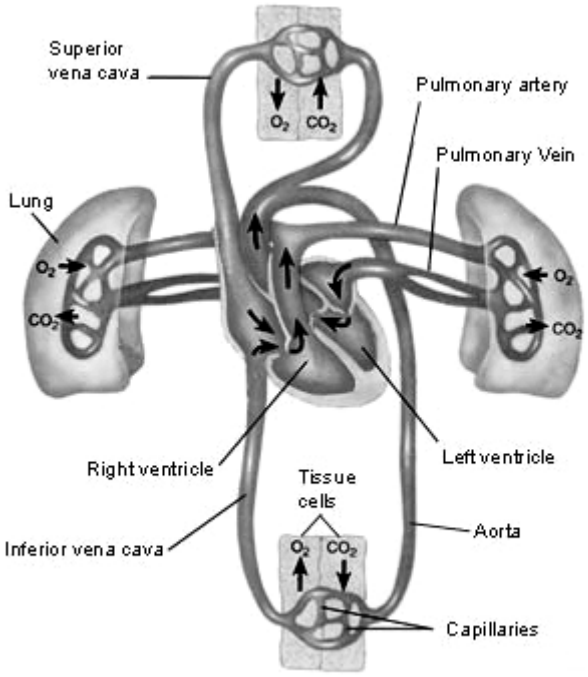

Fig 2.3 Pulmonary and systemic circulatory system [35]

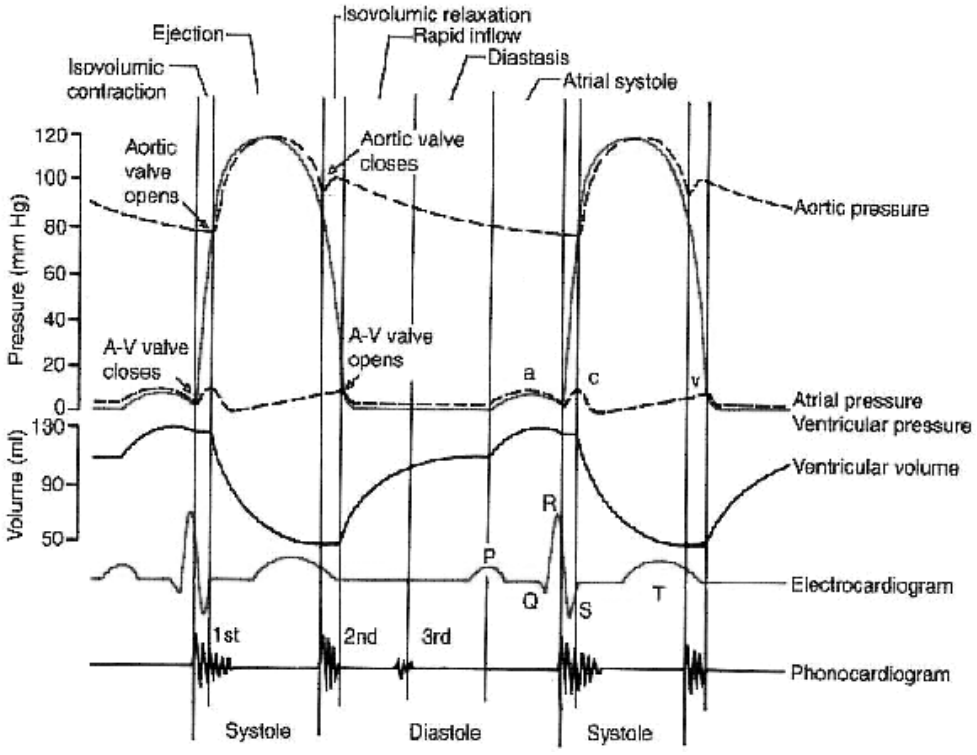

Fig 2.4 Events of cardiac cycle [24]

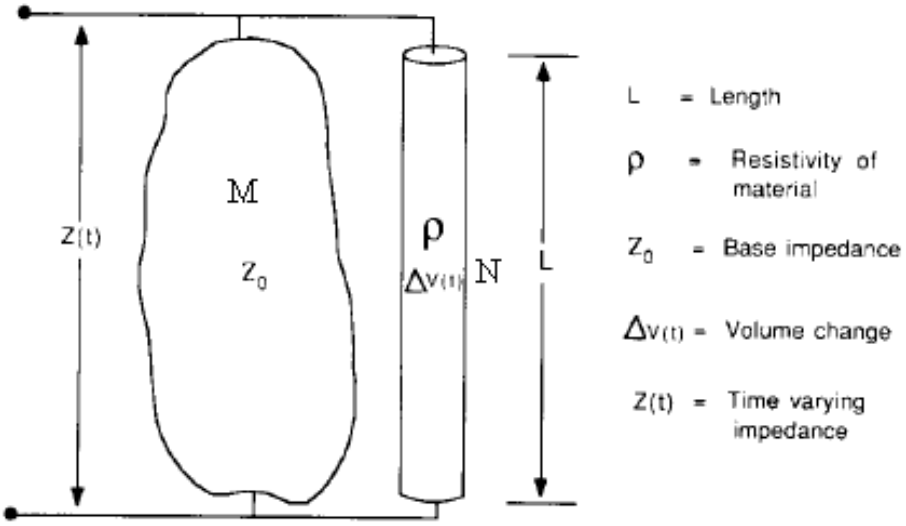

Fig 2.5 Kubicek parallel column model [3]

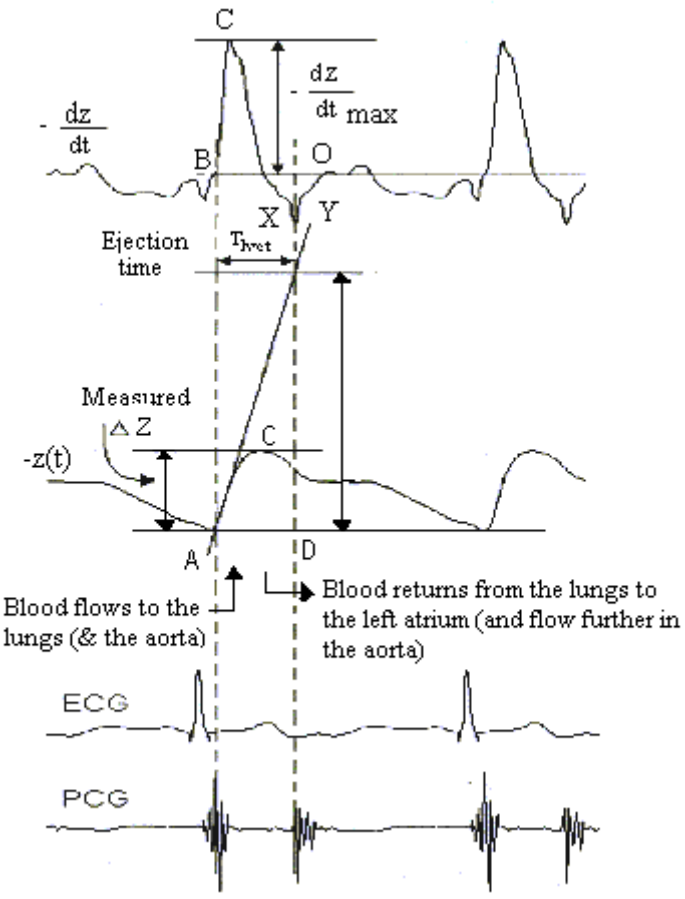

Fig 2.6 ICG waveform showing extrapolation technique [3]

Chapter 3
IMPEDANCE CARDIOGRAPH HARDWARE

3.1 Introduction

In the impedance cardiograph developed earlier at IIT Bombay [21] – [23], several improvements were needed. Mainly the DC cancellation circuit that was used to remove the offset from the extracted ICG was introducing its own oscillatory drift. The oscillator needed to be buffered and the entire circuit layout needed to be made more compact. Thus the main objective of this project was to improve the instrumentation for impedance cardiography based on the earlier design. The instrumentation was built and tested. The hardware consists of a Wein bridge oscillator, voltage to current converter, high skin-electrode contact indicator, ICG extraction circuit, DC cancellation circuit, and ECG amplifier. It is to be noted that the whole circuit is transformerless. The earlier design used a current source for excitation, with one of the terminals at virtual ground. It was decided to also provide a current source, with the two terminal voltages balanced with respect to ground in order to investigate improvements to be obtained by it. These two current sources will be referred to as "unbalanced" and "balanced" current sources respectively. Each of these hardware modules are explained in the following sections.

3.2 Oscillator

A Wein bridge oscillator has been used as the sinusoidal source [30][31]. The oscillator circuit, shown in Fig 3.1, generates a sinusoidal excitation of frequency f_o = 106 kHz with $C_2 = C_3$ = 100 pF, $R_4 = R_5$ = 15 kΩ, for nominal f_o = 100 kHz. The frequency was calculated using the equation $f_o = 1 / 2\pi RC$. The amplitude of the signal can be varied by the potentiometer R102 to a maximum of 8 Vp-p.

Since impedance sensing is done by amplitude demodulation, amplitude should be stable at the oscillator output. Amplitude stability is provided by controlling the gate bias

of FET T1. When the negative cycle of the output exceeds 1.4 V then the diodes D1 and D2 get forward biased and the excess voltage gets filtered out by the impedance network R1 and C1 at the gate of FET T1, thus providing it a negative bias. The negative bias at the gate increases the FET's channel resistance thus decreasing the overall gain of the oscillator. The excess negative voltage that is generated using the diode network should be in the linear region of the FET channel resistance vs gate bias characteristic.

The output of the oscillator is then buffered to the V/I converter. The output of the oscillator is given to the buffer through a jumper (JM1). This jumper can be configured in such a way that input to the V/I converter can also be given from an external signal generator to use a different excitation frequency. Potentiometer R102 is used to control the amplitude in order to set the excitation current.

3.3 Voltage to current converter

a) Unbalanced current source:

The circuit diagram of the voltage-to-current converter is shown in Fig 3.2. The excitation current is given as

$$I_{rms} = V_{rms} / R_7 \tag{3.1}$$

The current from the V/I converter is fed to the outer current injecting electrode pair I1 and I2 of the four-electrode configuration through DC blocking capacitors, with values being selected to provide a negligible impedance compared to the basal impedance of the thorax at the operating frequency. The V/I converter also has a 2.2 kΩ resistance in parallel with the excitation electrode path. This limits the dc voltage gain of the circuit and prevents the opamp from going into saturation in case of loose skin-electrode contact. In this current source, the electrode I1 is at virtual ground. Hence the two terminal voltages are unbalanced with respect to ground. This leads to the possibility of stray currents and common mode pick-ups. Transformer-based balanced excitation circuit has been reported to solve this problem [30]. In Kuriakose's dissertation [21], it was proposed to use a transformerless voltage-to-current converter, where two output terminal voltages at I11 and I22 are balanced with respect to ground. This circuit has been incorporated in the present design.

b) Balanced current source:

The circuit of the current source with output terminal voltages at I11 and I22 balanced with respect to ground is shown in Fig 3.3. The magnitude of current is set by the resistor R_{94}. The current is fed to the current injecting electrodes through DC blocking capacitors. In this circuit,

$$R_{91} = R_{92} = R_{99} \tag{3.2}$$

$$R_{96} = R_{97} \tag{3.3}$$

$$R_{93} = R_{91} \parallel R_{92} \parallel R_{99} \tag{3.4}$$

$$R_{98} = R_{97} \parallel R_{96} \tag{3.5}$$

Thus we get

$$V_z = -V_2 - V_x \tag{3.6}$$

$$V_y = -V_x \tag{3.7}$$

Let I be the current through R_{94} flowing from V_z to V_y

$$I = \left(\frac{V_z - V_y}{R_{94}} \right) \tag{3.8}$$

Let the net load in the current path between V_x and V_y be R_L.

From equations 3.6, 3.7, and 3.8, we have

$$I = -\left(\frac{V_2}{R_{94}} \right) \tag{3.9}$$

$$V_y = V_z - IR_{94} = V_z + V_2 \tag{3.10}$$

Also

$$V_y = V_x + IR_L \tag{3.11}$$

From equations 3.11, 3.7 and 3.9, we get

$$V_x = -0.5\left(\frac{R_L}{R_{94}} \right) V_2 \tag{3.12}$$

$$V_x = 0.5\left(\frac{R_L}{R_{94}} \right) V_2 \tag{3.13}$$

Thus we see that the two output terminals are balanced with respect to ground.

From equation 3.5, we have

$$V_z = V_I\left(\frac{1}{2}\frac{R_L}{2R_{94}} - 1\right) \tag{3.14}$$

For proper circuit operation, none of the outputs should go into saturation.

The jumper "JM2" provides the option for selecting either of these two current sources for ICG by proper configuration.

3.4 Contact impedance indicator

The contact impedance indicator circuit was designed to ensure proper contact of the electrode with the skin. As shown in Fig 3.4, the output of the V/I converter is rectified and low pass filtered to get the average voltage which is then compared with the half wave rectified average voltage of the oscillator. When the electrode contact is not proper with the skin, the average voltage of the V/I converter is more than that of rectified average voltage of the oscillator, so the comparator turns on the LED to indicate loose contact of the electrode with the skin. This comparison is done for both positive and negative cycles of the injected sinusoid. When both LED1 & LED2 are off, it indicates good contact of the electrodes.

3.5 ICG extraction circuit

The ICG extraction circuit has two major sections: (a) the instrumentation amplifier section and (b) the demodulator and filter section.

a) Instrumentation amplifier

This forms the first stage of ICG extraction circuit and basically formed by 3 opamps. The circuit is shown in Fig 3.5. The instrumentation amplifier provides a very high input impedance for picking up any differential signal. The very first stage of the amplifier has a high pass filter with cutoff of 16 kHz. By this any 50 Hz interference will be eliminated and only the 100 kHz modulated signal will be picked up by the amplifier. Further this filter also rejects any movement artifacts or ECG signal from being picked up. The differential gain of the amplifier is around 10. The gain of the differential amplifier can be got from the expression

$$\text{Gain} = \left(1 + \frac{2R_{f1}}{R_{i1}}\right)\left(\frac{R_{f2}}{R_{i2}}\right) \tag{3.15}$$

where $R_{f1} = R_{22} = R_{24}$, $R_{i1} = R_{23}$, $R_{f2} = R_{27} = R_{28}$, and $R_{i2} = R_{25} = R_{26}$

The opamp used is LF356 which has the input stage as FET and also it is internally frequency compensated. With the input stage being FET, the input bias current is in the order of Pico amperes. The output of this instrumentation amplifier is an amplitude modulated voltage signal whose modulation is proportional to the impedance change in the thorax. This is then fed to the demodulator circuit.

b) Demodulator and filter

Output of the instrumentation amplifier is capacitively coupled to the demodulator. This provides a high pass cut-off of approximately 534 Hz for the component values shown in Fig 3.6. The frequency is calculated using the expression

$$f = \frac{1}{2\pi C_{18}\left(R_{29} \parallel R_{30} \parallel R_{31}\right)} \tag{3.16}$$

The demodulator consists of a full wave precision rectifier or detector followed by a low pass filter to remove the 100 kHz carrier signal. The circuit is shown in Fig 3.6. The detector circuit uses opamp LF356 and switching diodes IN4148 which provide acceptable results at 100 kHz. The rectified output is low pass filtered formed by R_{35} and C_{20}, with a 3 dB cutoff at 30 Hz. It smoothens the rectified signal and also filters out the 50 Hz pick-ups. The output of the filter is then simultaneously fed to the DC cancellation circuit to get the $z(t)$ waveform and to low pass filter to get Z_o. The low pass filter to get the Z_o has a very low cut off of 0.8 Hz so as to remove the respiratory artifacts.

3.6 DC cancellation circuit

In acquisition of bio-signals, usually the signal of interest is of very small amplitude and is often corrupted by slowly varying (low frequency) artifacts. Further in the process of amplification, drift gets introduced. The net slowly varying component can be filtered out using a high pass filter of very low cut-off. But often it is very difficult to achieve this using analog filtering. It may be possible to employ digital filtering, but the drift needs to be at least partly removed before A/D conversion in order to make proper use of ADC range.

To overcome this problem a drift cancellation circuit can be used, making use of the fact that the signal occupies a certain range and crossing the range is an indication of drift. In this circuit, two comparators are used to set two thresholds. Whenever the signal after amplification crosses this threshold, it is pulled back in this range by subtracting a voltage. It is to be noted that output signal is not suitable for processing during the signal correction. Thus the correction interval has to be indicated as an output along with the amplified biosignal.

Our circuit is based on the circuit given earlier by Zhang et al [6], using a successive approximation register and D/A converter, as schematically shown in Fig 3.7. Whenever the voltage V_o crosses the threshold range (V_{t1},V_{t2}), the successive approximation register (SAR) starts changing and the DAC gives the corresponding analog voltage which is subtracted from the input voltage. This correction is repeated thus keeping the signal within the range defined by the two thresholds. A simpler version was developed later by Joshi [22][33], using an integrator replacing the SAR and DAC as shown in Fig 3.8. However a serious problem of this circuit is that when the corrected output is well within the two thresholds and the integrator has no input, the integrator output changes due to leakage of charge on its capacitor. This results in a self introduced drift in the output. Cancellation of this drift results in a slowly varying triangular oscillatory drift. To overcome this problem a microcontroller based circuit is developed. The successive approximation logic is firmware implemented in the microcontroller. Further in place of using an external D/A converter, a PWM output from the microcontroller is used for drift correction. The frequency of the PWM carrier was kept at 7 kHz.

The circuit is shown in Fig 3.9. The two different thresholds are set using a resistive network. Whenever the signal after amplification crosses these thresholds, a correction voltage is subtracted bringing back the signal to the middle of the two thresholds. The upper threshold is kept at –1 V and the lower threshold at –2.5 V and so the difference between the threshold voltages being 1.5 V. Whenever the signal crosses the upper threshold an additional, 0.75 V is subtracted from the signal. This constant voltage can be generated by changing the duty cycle of the PWM in steps. The SAR logic can be simplified by just calculating the value that corresponds to an increase in duty cycle of the PWM to generate an average voltage of 0.75 V after being low pass filtered. Similarly when the signal crosses the lower threshold, the duty cycle is changed so that

the average voltage being subtracted is reduced by 0.75 V. The flow chart of the program used is given in Fig 3.10.

However to increase the range of correction, a potentiometer R38 was introduced. By adjusting the value of this potentiometer, the averaged DC output of the low pass filter for each minimum increase in duty cycle of the PWM can be amplified appreciably to a very high value. Thus a maximum of 256 step increase of PWM, each step corresponding to 0.75 V can be incorporated. The low pass filter used is of second order which eliminates the PWM carrier at the output making the drift cancellation more stable. The correction period of the drift cancellation circuit was found to be ≈ 10 ms and it was working satisfactorily up to signal frequency of 10 Hz. This can be further improved by increasing the PWM carrier frequency which can be achieved by operating the microcontroller at a higher clock and by optimizing the program.

3.7 ECG amplifier

The ECG amplifier is a part of the impedance cardiograph and is used to acquire the ECG simultaneously with the ICG signal. This ECG signal is used as a fiducial mark for ensemble averaging of the ICG signal to calculate the cardiac output as shown in the Fig 2.6. There are two ECG amplifiers incorporated in the hardware. Both the ECG amplifiers are same in construction. One ECG amplifier is connected to the voltage pickup electrodes E1 and E2 of the ICG extraction circuit. The filter section in the instrumentation amplifier section eliminates the ICG signal from being picked up by this amplifier. The second ECG amplifier is provided to record ECG from limb electrodes.

The circuit diagram of the ECG amplifier is shown in the Fig 3.11. The low pass filter cut-off was kept at 22 Hz and the high pass filter cut-off was kept at 1.6 Hz. The portion of signal which is of interest to ICG is the QRS complex, which falls well with in this pass band.

3.8 Four-electrode configuration

Basically for impedance measurements in human body, there are two types of electrode configuration used: 2-electrode and 4-electrode configuration. In 2-electrode configuration, the voltage sensing electrodes are the same as the current injecting electrodes. In 4-electrode configuration, the current injecting and voltage sensing

electrodes are different. The equivalent resistor network of 4-electrode configuration used for our application is shown in Fig 3.12 [21].

The outer two electrode pairs I1 and I2 are used for current injection and the inner ones E1 and E2 are used for voltage pickup. The impedance Z_a and Z_b come in the path of injected current. The impedance Z_x is varying and thus the voltage V_{zx} is proportional to this impedance change. To measure this $V_{zx,}$ the amplifier should have a very high input impedance. Suction cup electrodes are used for both current injection and voltage pick-up. The choice of suction cup is the ease to place the electrode in a position where the movement artifact would be very less. Also chest belts are designed and prepared to hold these suction cup electrodes in position. The electrodes are dipped in gel before connecting it to body to ensure proper contact with the skin.

3.9 PCB design

The impedance cardiograph circuit was assembled on a double sided epoxy PCB with the size of the board 10 mm × 16.5 mm. Care was taken to isolate the oscillator module from rest of the circuit by providing an isolation of 3 mm (copper free). All the connectors used are PCB mountable in order to reduce external noise pick-up. The connectors used are RCA type in order to provide good shielding for the signals from and to the patients. Test pins are provided at various points for on-board testing of various modules. Decoupling capacitors are provided at all places were the power line track is changing the side in order to by-pass high frequency components.

The analog and digital grounds are separated and joined at the most optimum point. The ground plane is formed on the component side and the power and signal tracks on the solder side. The crystal used for the microcontroller is shielded to avoid interference. The PCB was enclosed in a box whose dimensions are 18.5 × 13 × 3.5 cm. The component layout and track layout of the PCB is shown in Appendix D and the orthogonal view of the box is shown in Appendix E.

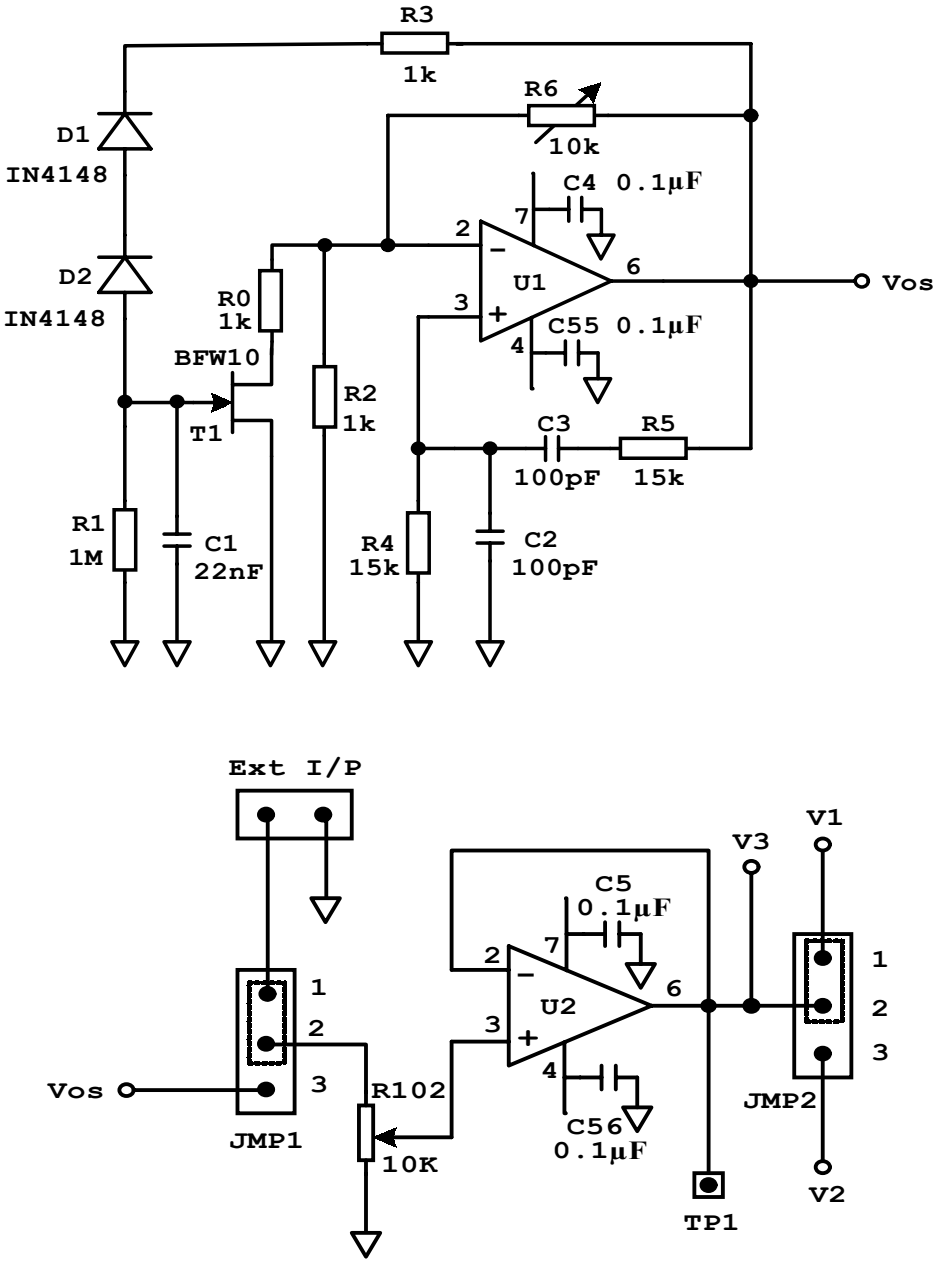

Fig 3.1 Wein bridge oscillator with buffer
(U1, U2: LF356)

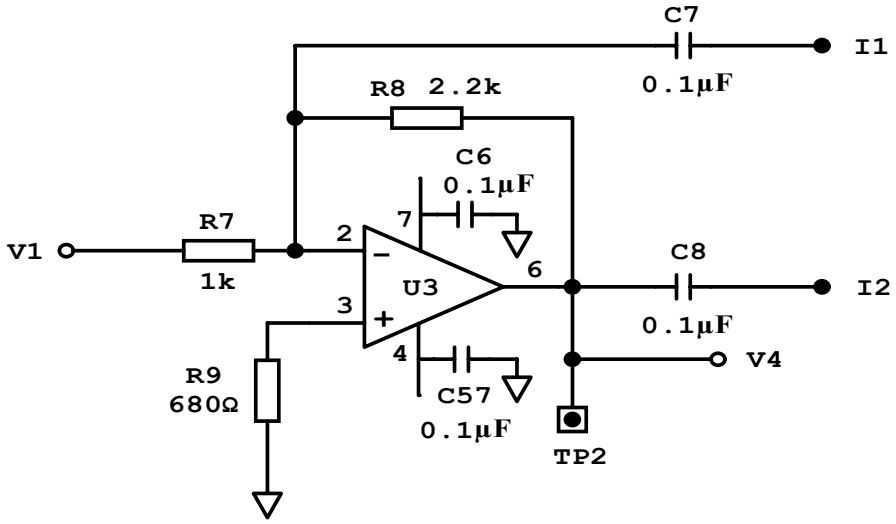

Fig 3.2 Unbalanced current source

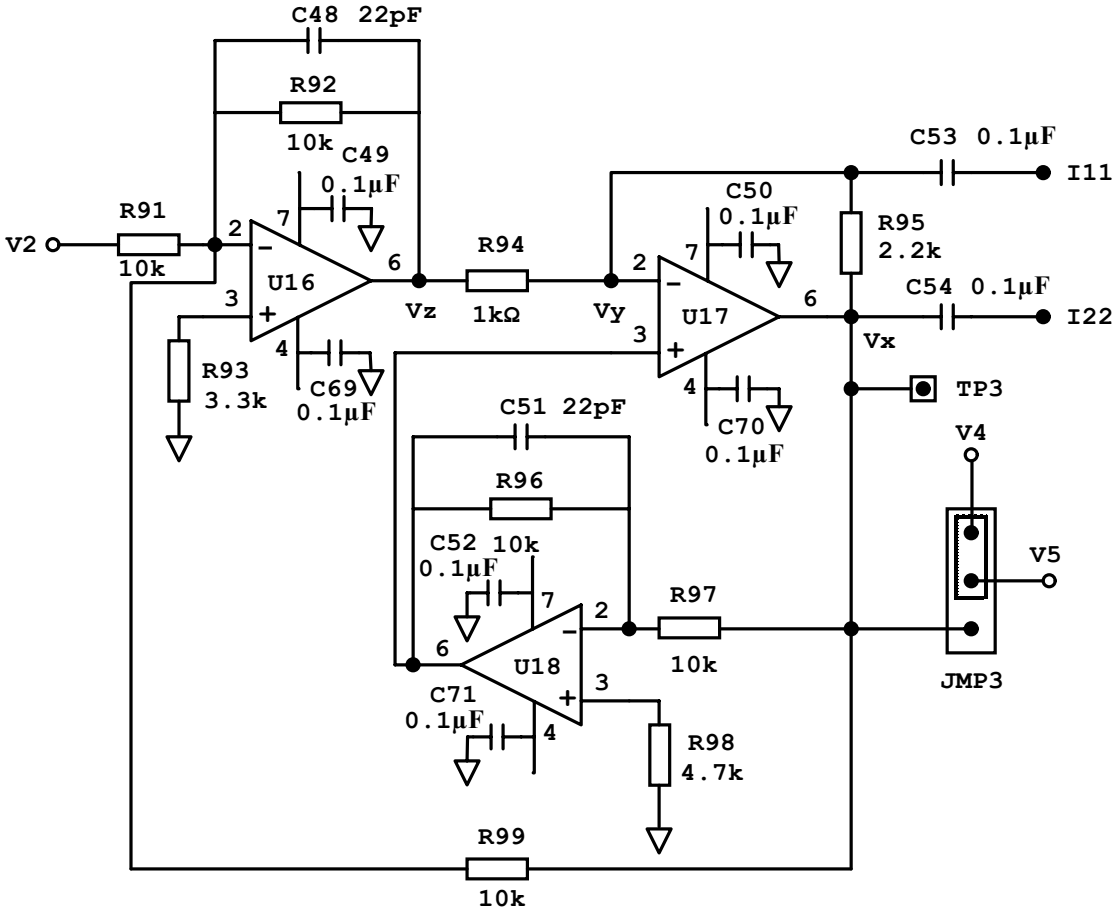

Fig 3.3 Balanced current source
(U3, U16, U17, U18: LF356)

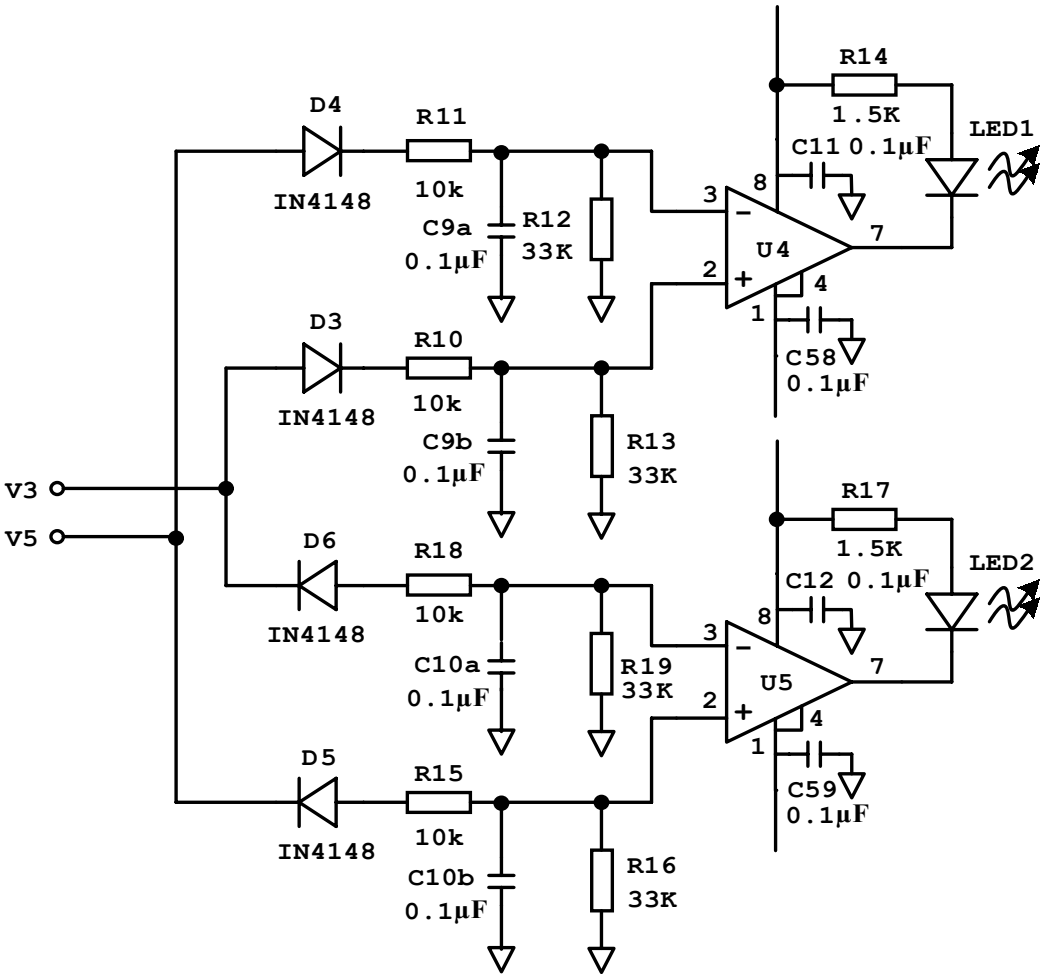

Fig 3.4 Contact impedance indicator
(U4, U5: LM311)

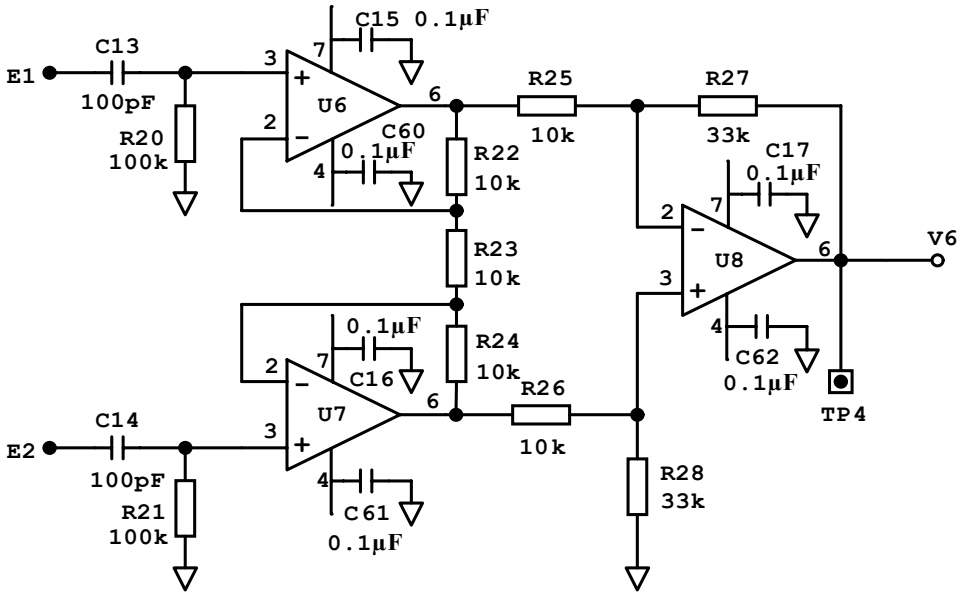

Fig 3.5 Instrumentation amplifier section of ICG circuit

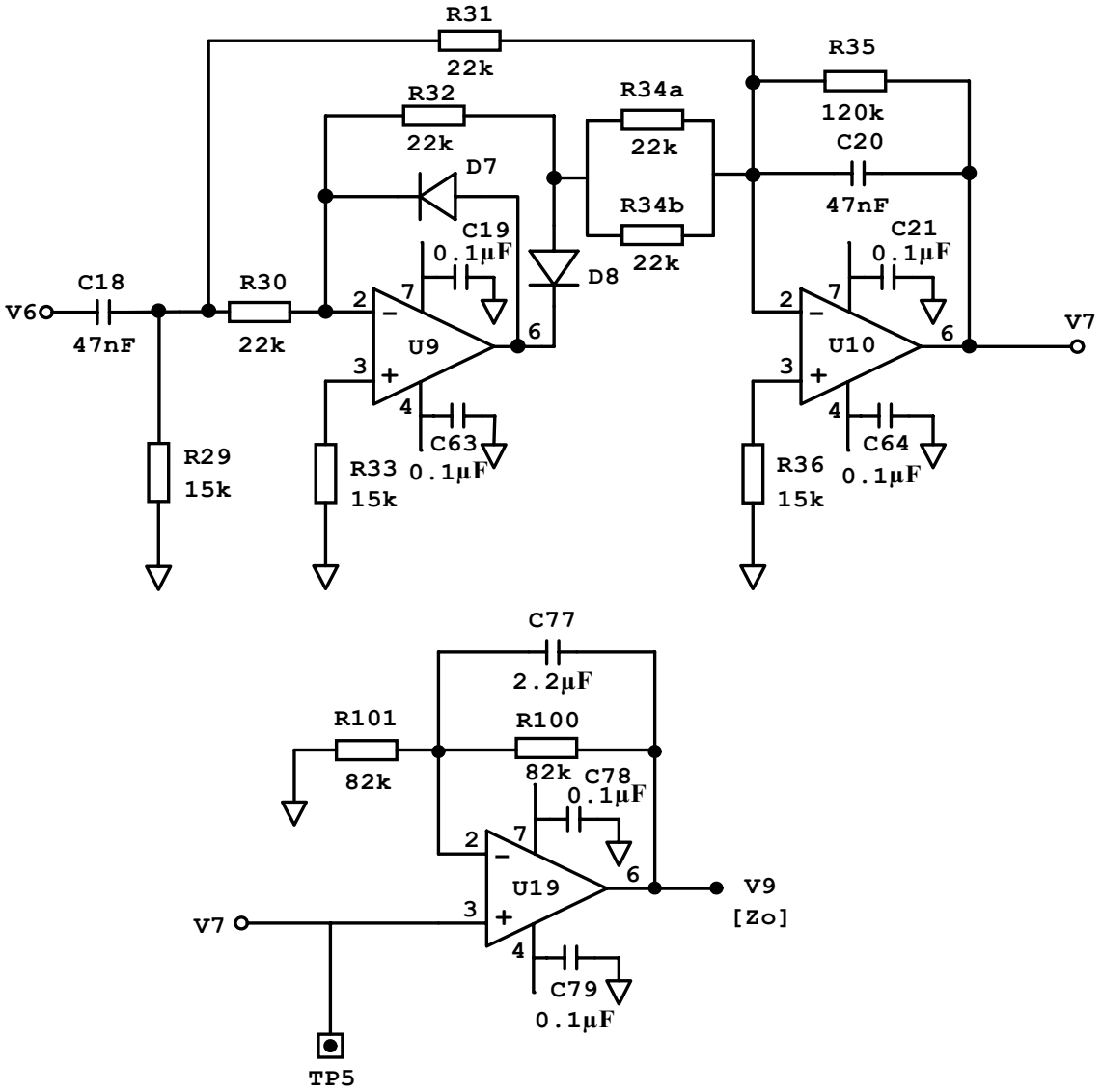

Fig 3.6 Demodulator and Z_o extraction section of ICG circuit
(U6, U7, U8, U9, U10, U19: LF356)

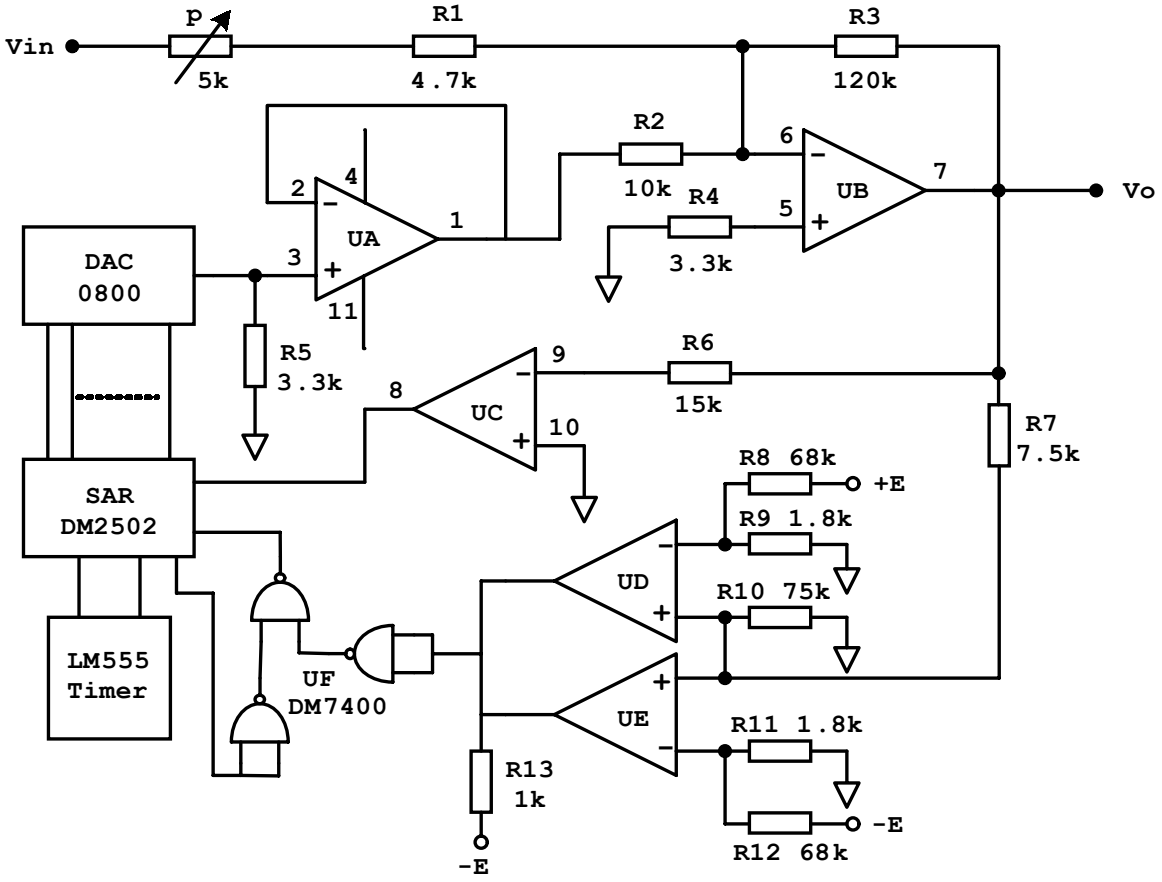

Fig 3.7 Drift cancellation circuit developed by Zhang et. al [6]
(UA, UB: LM741; UC, UD, UE: LM319)

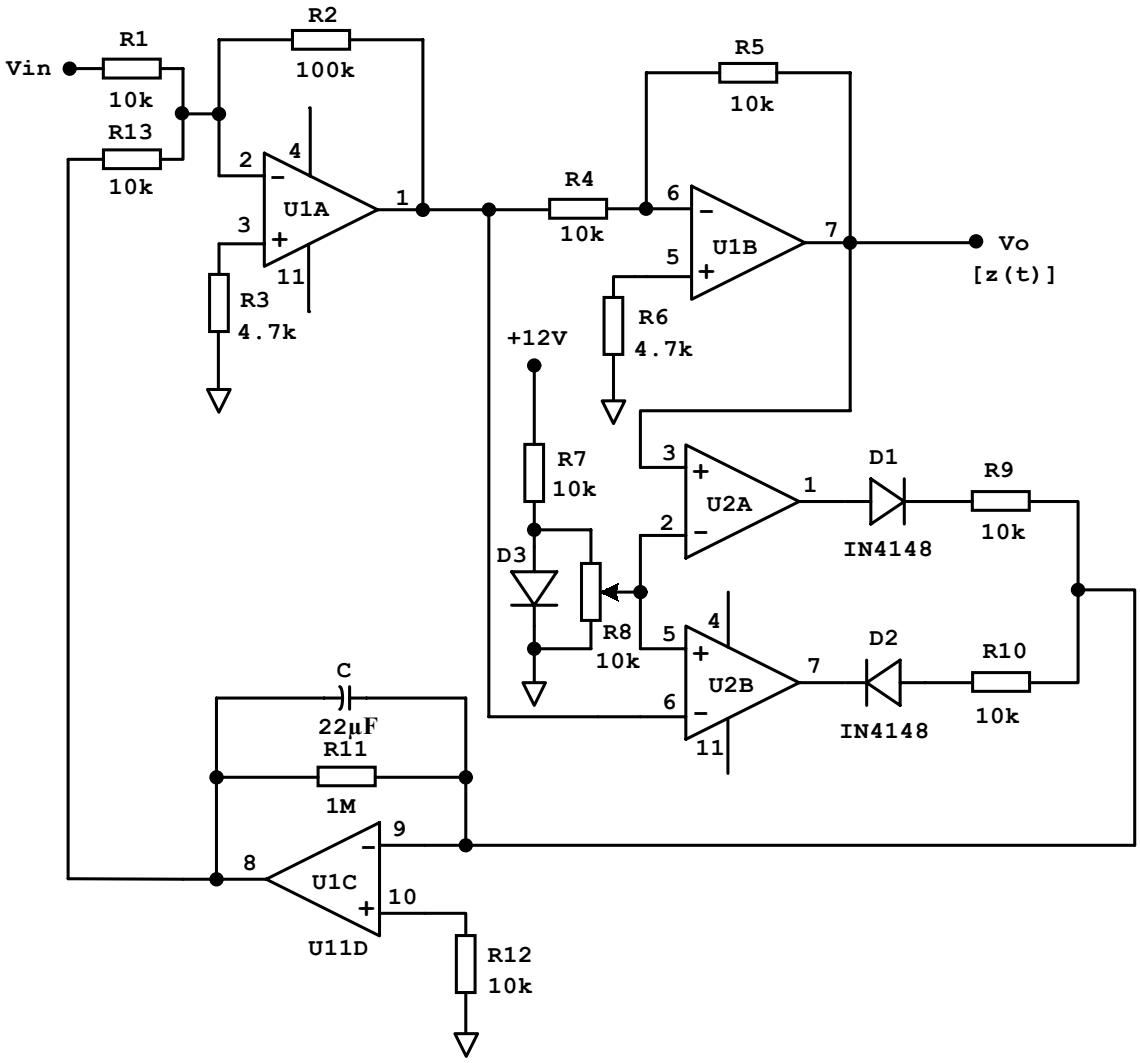

Fig 3.8 Drift cancellation circuit developed by Joshi [33]
(U1, U2: LM324)

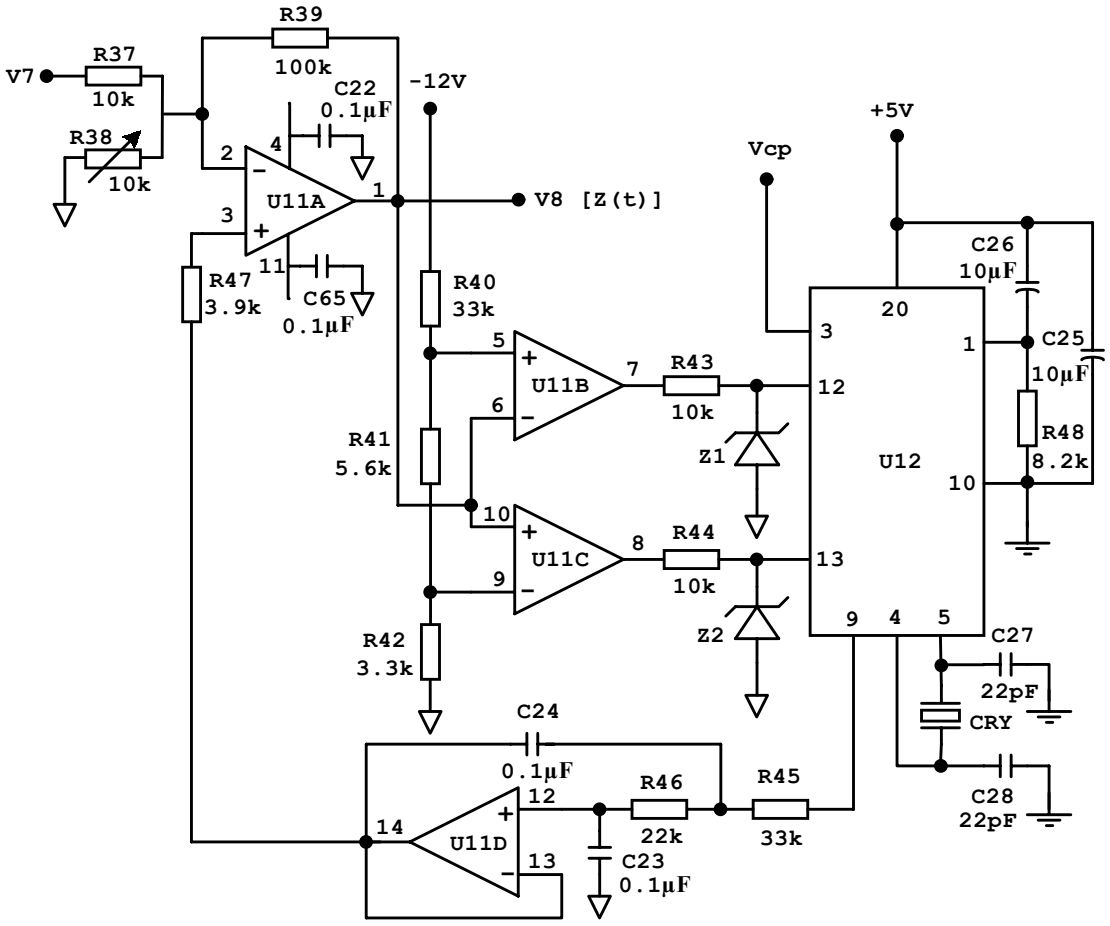

Fig 3.9 Circuit diagram of the PWM based drift cancellation circuit
(U11: TL084, U12:AT89c2051)

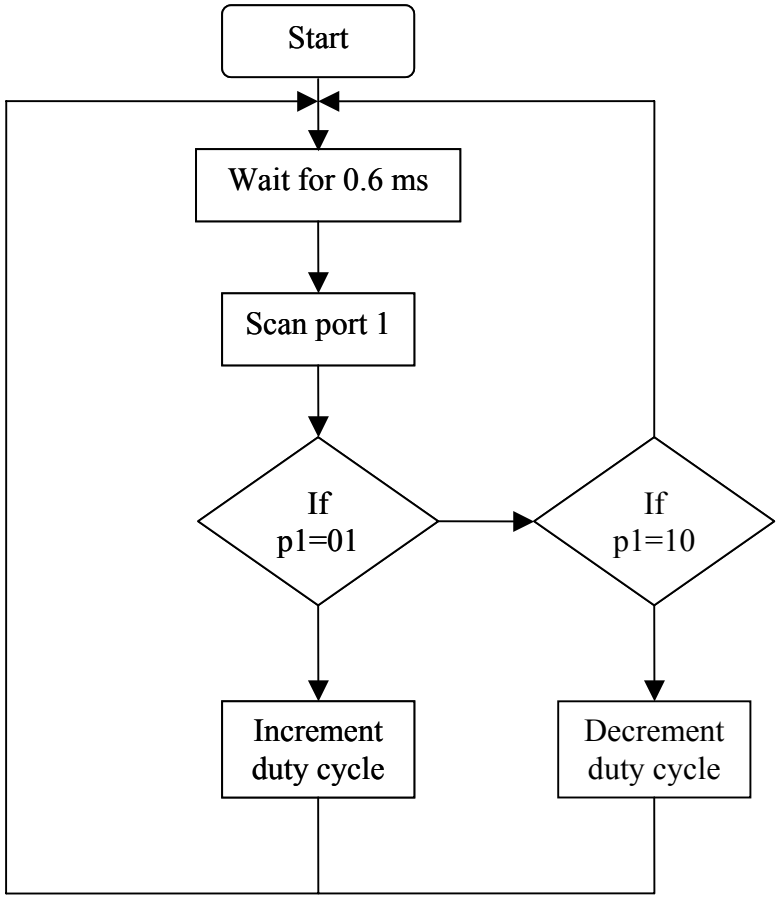

Fig 3.10 Flow chart for program of DC cancellation circuit

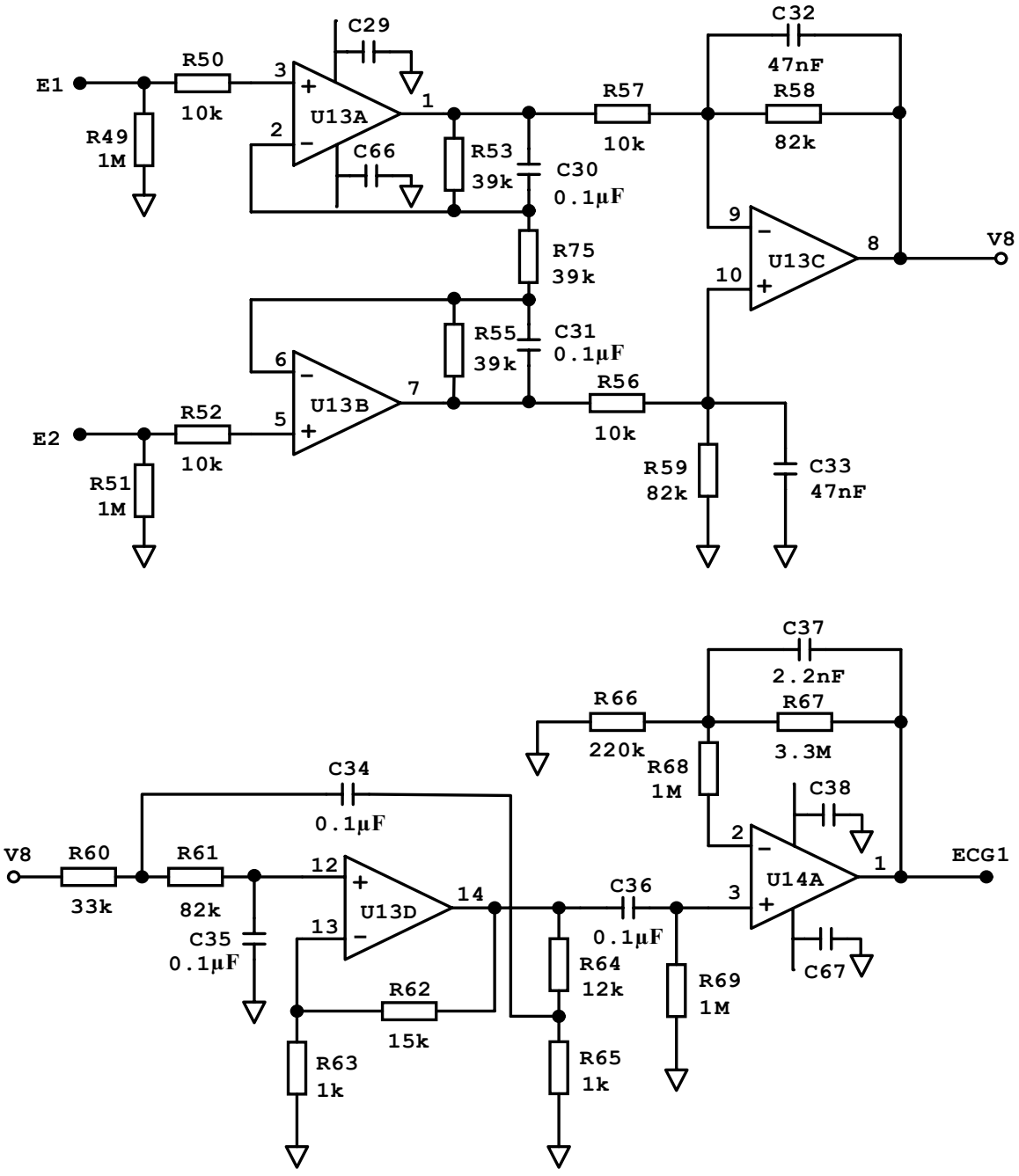

Fig 3.11 a) Circuit diagram of ECG amplifier with input from E1 & E2

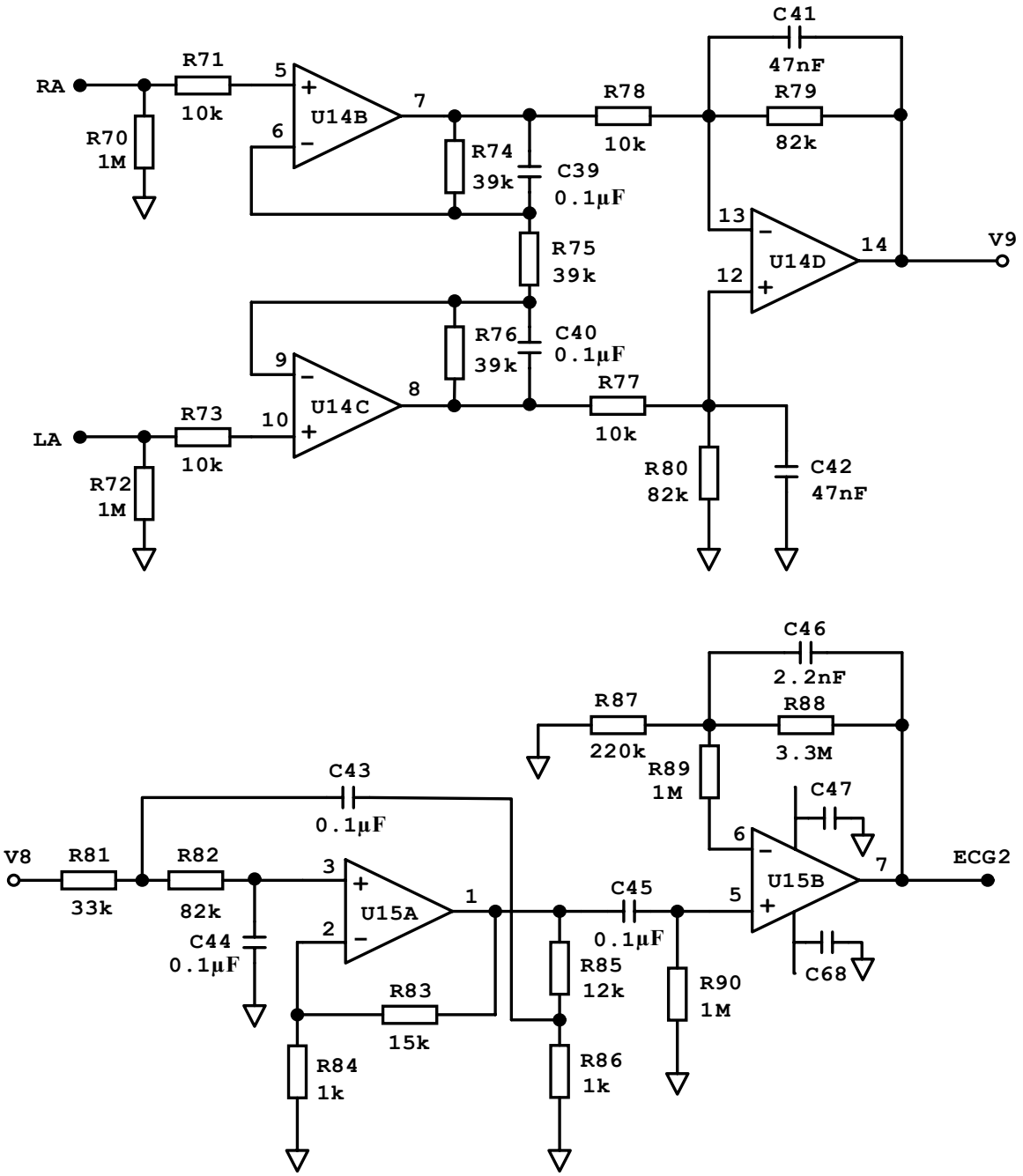

Fig 3.11 b) Circuit diagram of ECG amplifier with input from limb electrodes
(U13, U14, U15: TL084)

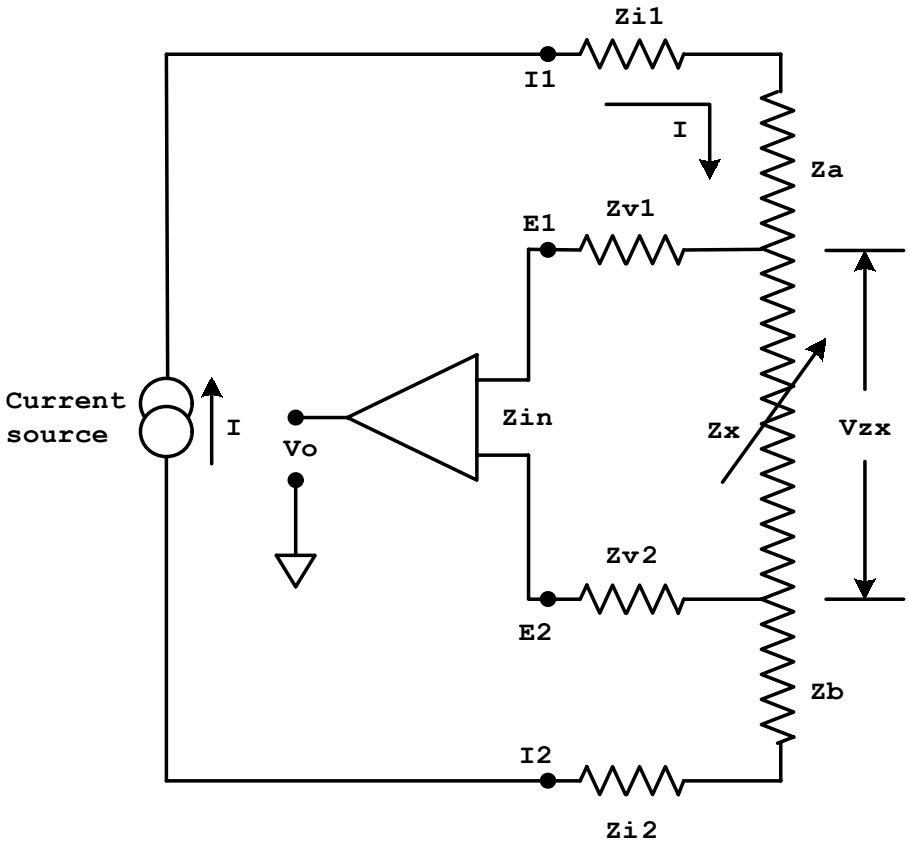

Fig 3.12 Four-electrode configuration [21]

Chapter 4
THORACIC IMPEDANCE SIMULATOR

4.1 Introduction

As part of instrumentation development for the impedance cardiography, a thoracic impedance simulator has been developed based on an earlier design by Kuriakose [21]. This simulator is used for comprehensive testing and calibration of the impedance cardiograph instrument to ensure proper signal pick-up and detection of impedance variation. It has the facility for varying the beat rate, magnitude of common and differential mode ECG signals and a fixed percentage variation in the thoracic impedance as a square wave. Option for feeding external pick-ups is also incorporated. The simulator can be operated either through a battery or an external power supply.

4.2 Thoracic impedance simulator model

An impedance model of the thorax, used in the simulator for the 4-electrode measurement setup is shown in Fig 4.1. The high frequency current is injected through the inputs I1 and I2. The variation of the impedance can be measured through the output E1 and E2. In this model, R_es constitute the tissue-electrode contact resistances for 4-electrode configuration. Resistances R_O and R_S are the parallel column model resistances and R_{S1} and R_{S2} are the fixed resistances in the current path. Option for feeding external pick-up is denoted by V_p and the resistance in the pick-up path by R_p. The voltage sources V_{ed} and V_{ec} represent the common mode and differential mode ECG signals respectively. A very simplified simulation of the variation in the thoracic impedance is used here. The net resistance, switches between R_O and $R_S \parallel R_O$ in response to cardiac systole pulses. This pulsating change in the resistance is useful for calibration of the impedance detector unit.

4.3 Model relations with the schematic

The thorax model of Fig 4.1 has several sources without a common node. These are difficult to realize in an electronic circuit without using transformers. In order to have an easily realizable circuit, the model can be modified to a schematic shown in Fig 4.2. Relations of the component values in the schematic of Fig 4.2 to those in the model of Fig 4.1 are as the following

$$R_1 = R_{s1} + R_{e1} \tag{4.1}$$

$$R_2 = R_{e2} \tag{4.2}$$

$$R_4 = R_{e4} + R_{s2} \tag{4.3}$$

$$R_3 = R_{e3} \tag{4.4}$$

$$R_{y1}' = R_{y1} \parallel \left(R_z + \left(R_{y2} \parallel R_{x2}\right)\right) \tag{4.5}$$

$$R_{y2}' = R_{y2} \parallel \left(R_z + \left(R_{y1} \parallel R_{x1}\right)\right) \tag{4.6}$$

$$V_1 = V_{x1}\left[\frac{R_{y1}'}{R_{x1} + R_{y1}'}\right] = V_{ec} + \frac{V_{ed}}{2} \tag{4.7}$$

$$V_2 = V_{x2}\left[\frac{R_{y2}'}{R_{x2} + R_{y2}'}\right] = V_{ec} - \frac{V_{ed}}{2} \tag{4.8}$$

$$R_a = R_b = \frac{R_s}{2} \tag{4.9}$$

$$R_z = R_o \tag{4.10}$$

4.4 Building blocks of the simulator

The circuit development for the schematic of Fig 4.2 is shown in Fig 4.3 and is described below. The impedance switching is realized using a quad analog switches in IC 4066. The heart beat and CM/DM ECG generation is done using an astable multivibrator and inverter. There is small circuit for obtaining Vcc+ and Vcc– from a single supply.

Thorax impedance simulator

The circuit diagram of the thorax impedance simulator is shown in Fig 4.3. The 4 analog switches in IC CD4066 are paralleled together for a reduced "on" resistance. Switching in ICG mode results in approximately 1% variation in the base impedance.

$$R_{eq(on)} = R_z \,||\, (R_a + R_b + R_{s(on)}) \,||\, ((R_{x1} \,||\, R_{y1}) + (R_{x2} \,||\, R_{y2})) \tag{4.11}$$

$$R_{eq(off)} = R_z \,||\, (R_{y1} + R_{y2}) \,||\, (R_a + R_b + R_{s(off)}) \tag{4.12}$$

Taking $R_{x1} >> R_{y1}$, $R_{s(on)} << (R_a + R_b)$ *and* $R_{x2} >> R_{y2}$, we get

$$R_{eq(on)} = R_z \,||\, (R_a + R_b) \,||\, (R_{y1} + R_{y2}) \tag{4.13}$$

Taking $R_{s(off)} >> R_z$, we get

$$R_{eq(off)} = R_z \,||\, (R_{y1} + R_{y2}) \tag{4.14}$$

CD4066 analog switch have typical on-resistance of 120 Ω (for $V_{DD} - V_{SS} \approx 10$ V). After assembly of the circuit, measurements were made. Putting the values of Fig 4.3 in equation 4.12 and 4.14 we get,

The base impedance when the switch was "off" is $R_{eq(off)}$ = 19.8 Ω.

The impedance when the switch was "on" is $R_{eq(on)}$ = 19.6 Ω.

So a change in impedance of 0.2 Ω was simulated using this impedance simulator.

Heart beat generator

An opamp TL084 operated under astable multi-vibrator mode is used as a heart beat generator. The frequency of the multi-vibrator (heart beat rate) can be varied by adjusting the potentiometer Rpf (Fig 4.4). The beat rate is variable from 0.4 – 5 Hz (24 – 300 beats/min). The output of the heart beat generator can be given to CM/DM or simulator using the switch S1.

CM / DM ECG generator

The output of the heartbeat generator is given to the CM/DM ECG generator. An opamp TL084 is used for this purpose. A switch "S2 " is provided which selects either common mode or differential mode operation. The magnitude of CM/DM can be varied by using the potentiometer Rpg (Fig 4.4). The magnitude of CM is variable from 0 –

60 mV with < 1 mV differential signal in it. The magnitude of DM is variable from 0 – 20 mV with < 2 mV common mode signal in it. Offset null adjustment can also be taken care by adjusting the potentiometer Rpo.

ECG/ICG mode operation

The thorax simulator is used for calibration of the ECG amplifier and the ICG extractor, one at a time. Hence it is designed to be operated in one of the two modes: ECG or ICG mode. Both the ECG and ICG signal are square pulse taken from the heart beat generator. The switch S1 (Fig 4.4) is used to select either of these modes. In the ICG mode, the impedance change is got as a fixed percentage variation of the basal impedance Z_o.

Split power supply

The simulator can either be powered through a battery or an external DC power supply. The first stage of the simulator is the split power supply. The battery or the external DC source is connected to this split circuit. This split power supply constructed with an opamp (TL084) converts the single ended DC voltage of V_B to dual voltages of $V_B/2$ DC. The circuit should be operated by a 9 – 12 V regulated DC. All the circuits of the simulator are powered from this split supply. The circuit diagram of the split power supply is shown in the Fig 4.5.

Simulator with multi basal impedances

The hardware construction of this is same as that of simulator discussed above except the thoracic impedance simulator circuit. Generally the basal impedance of thorax may vary in the range of 19 – 30 Ω for various persons due to their physiological structure [3][4]. So a variable basal impedance has been incorporated in the simulator. Also the variation in the basal impedance due to the heart activity is kept from 1% – 2% in three steps (1, 1.7, & 2%). When the base impedance was fixed at 33 Ω, the decrease in it was 0.8 Ω and 0.6 Ω for various positions of switch S3 and S4. The base impedance can also be fixed at 32.2 Ω and 32.4 Ω by S3 and S4. All the controls are provided externally through switches, which can be operated manually. The control of these manual switches are given through analog switches to the circuit, which in turn control the functions of the simulator in various mode. By this, it is possible to avoid any external

noise picked up by the manual switches from corrupting the actual signal. The circuit diagram of the simulator is shown in Fig 4.6 and the CM/DM generator in Fig 4.7.

4.5 Operation and testing

The simulator can be operated in two different modes: ECG and ICG modes. These modes can be selected by the switch S1. In ECG mode again, we can have either common mode ECG or difference mode ECG. This can be selected using switch S2. When the circuit is in ICG mode, the switch S3 and S4 can be used to select the various basal impedances. In the ECG mode, the amplitude of the ECG signal in common mode is variable over 0 – 60 mV and the differential signal present in it is < 1 mV. In the ECG difference mode, the amplitude is variable over 0 – 20 mV and the common mode signal present in it is < 2 mV.

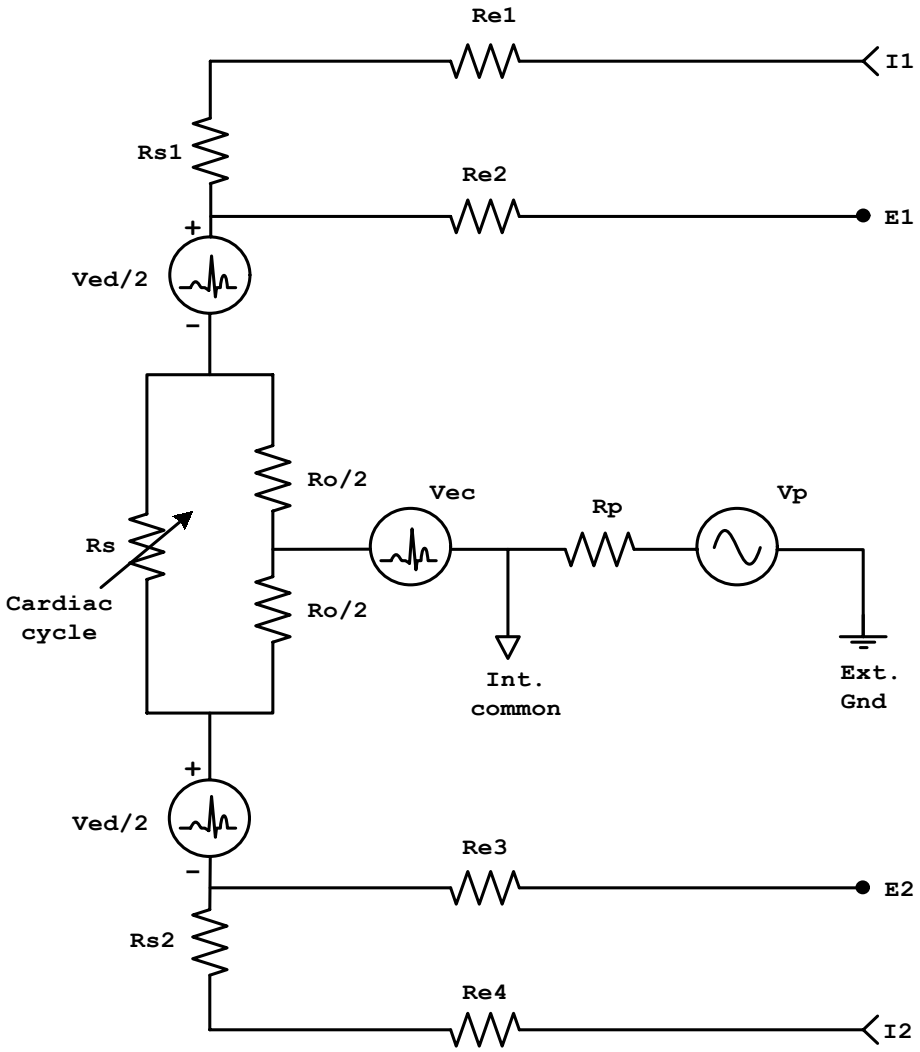

Fig 4.1 Thoracic impedance model

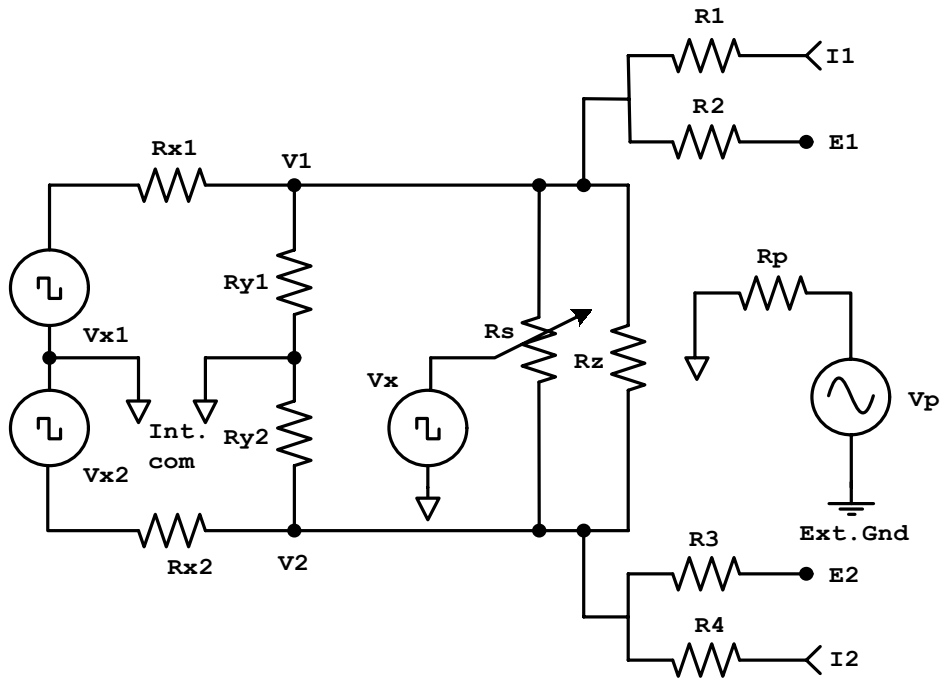

Fig 4.2 Schematic of the model shown in Fig 4.1

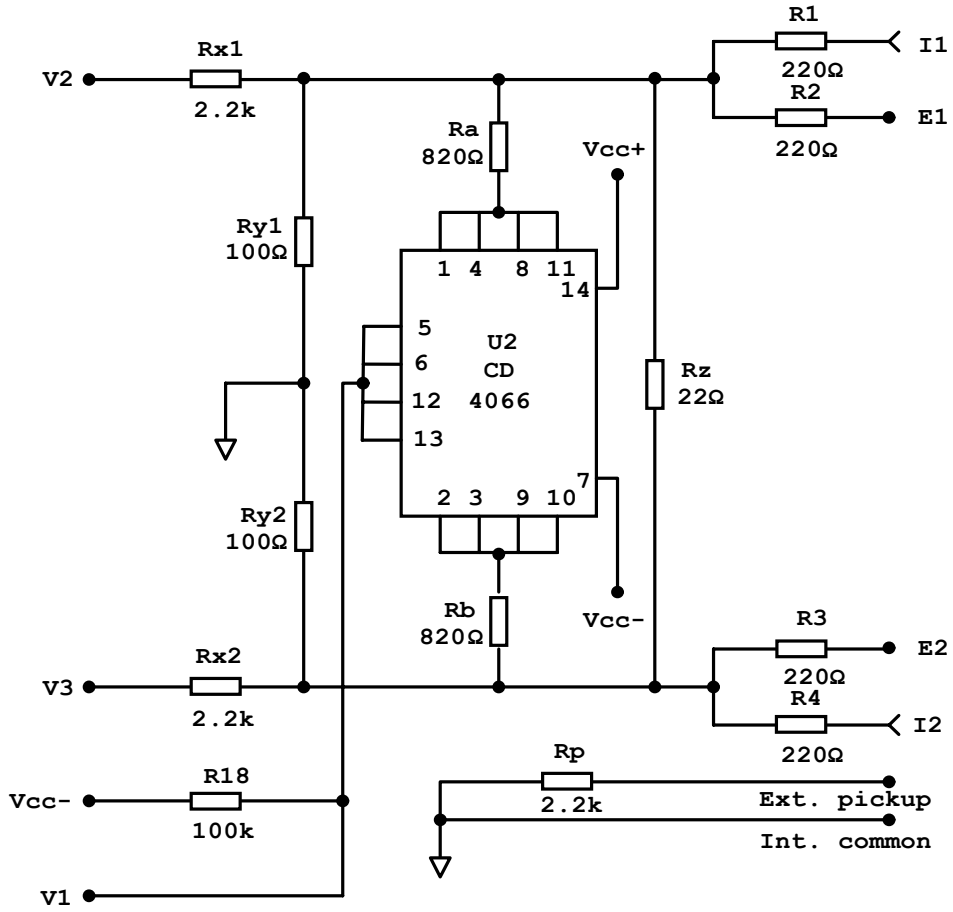

Fig 4.3 Circuit diagram of thoracic impedance simulator

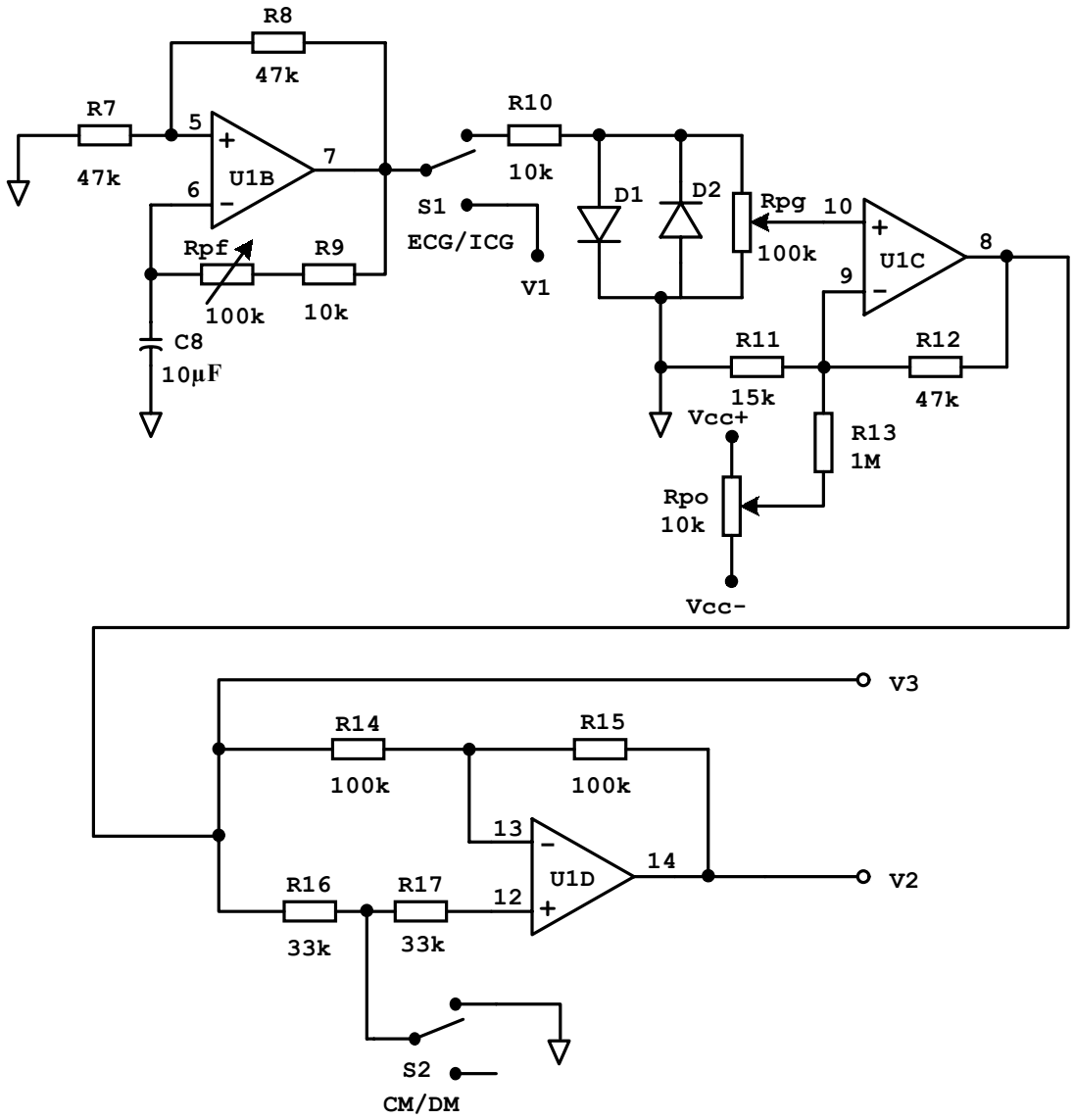

Fig 4.4 Circuit diagram of heart beat and CM/DM generator

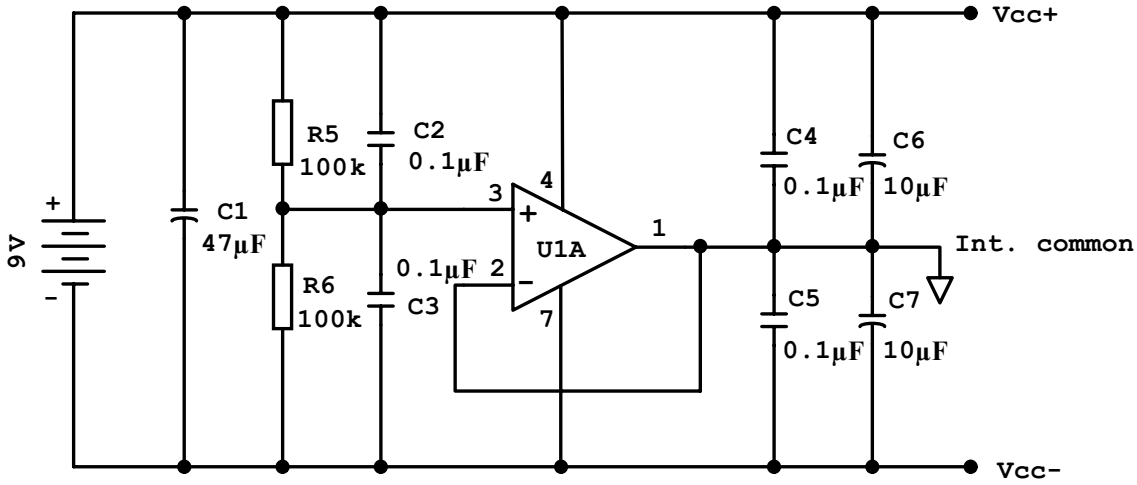

Fig 4.5 Split power supply
(U1: TL084)

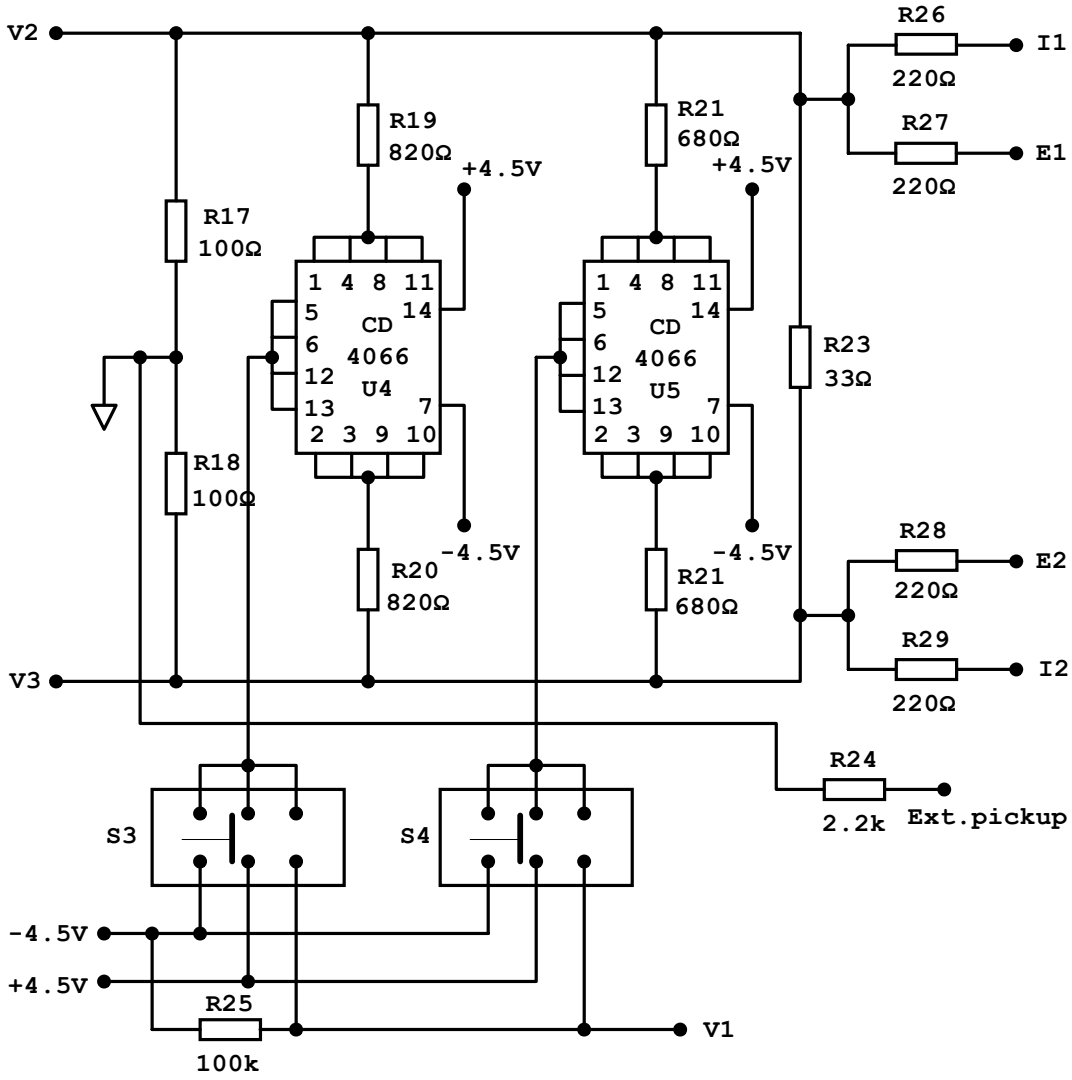

Fig 4.6 Circuit diagram of multi-basal thoracic impedance simulator

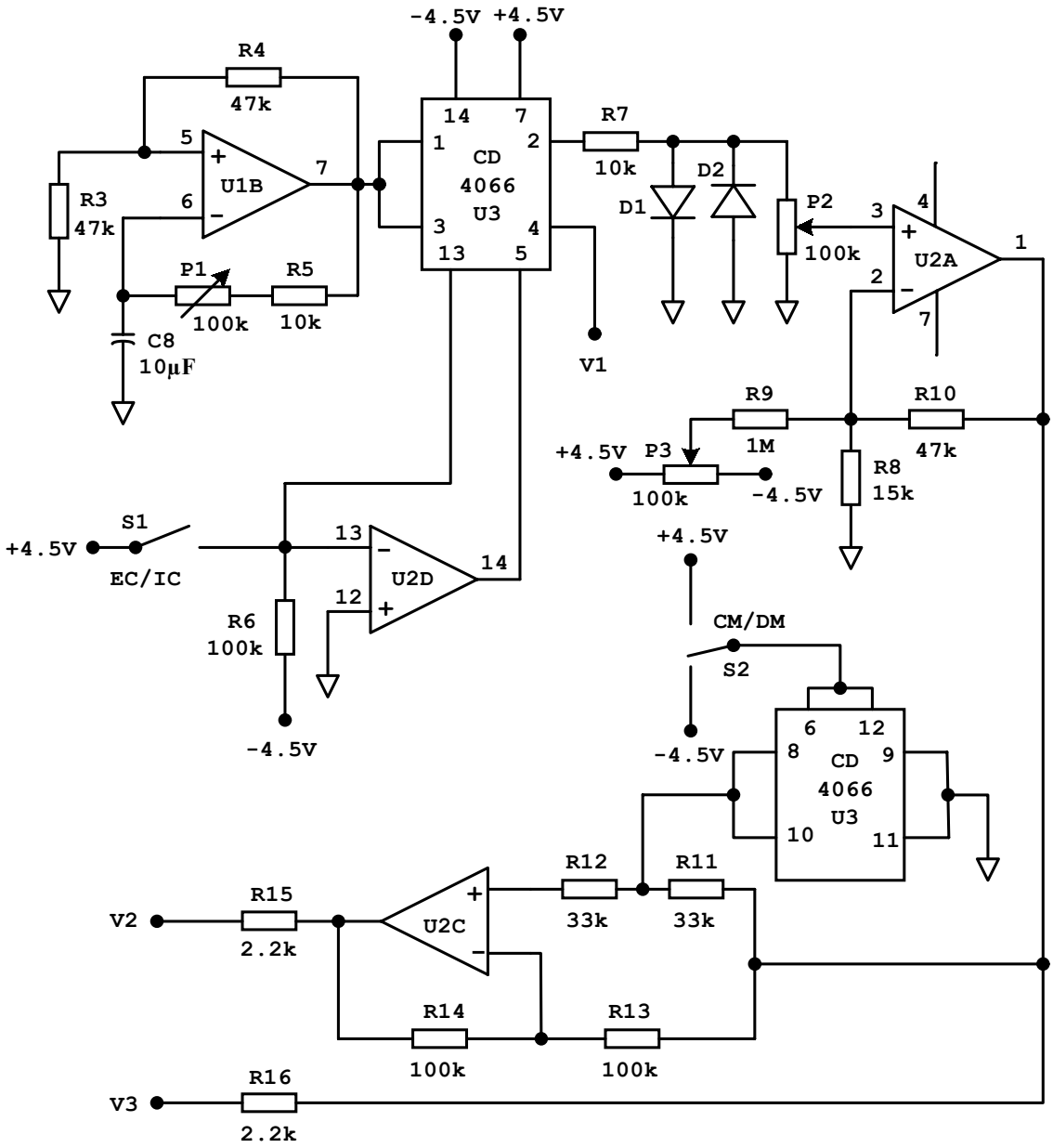

Fig 4.7 Circuit diagram of CM/DM generator for multi-basal thoracic impedance simulator (U1, U2: TL084)

Chapter 5
VALIDATION OF THE HARDWARE

The hardware developed was tested section wise under various conditions using test signals to validate its functions. All the testing were done at room temperature and with the opamps powered at ±12 V and microcontroller at +5 V DC.

5.1 Oscillator

The oscillator circuit of Fig 3.1 was tested for different resistive loading and the response was observed. The short time and long time amplitude stability of the oscillator was also monitored. Amplitude stability is necessary because this sinusoid used for excitation results in amplitude modulated voltage due to impedance variation. If the amplitude of the sinusoid is not stable then after demodulation this variation in amplitude will get reflected in the actual ICG signal thus corrupting it.

a) Short time stability

The output was observed using a DSO (Tek. TDS 5054, 5 G samples/s). The output was a sinusoid with its frequency varying between 91.7 – 92 kHz. The positive peak was found to be varying between +4.13 V to +4.26 V and this variation was very frequent. The negative peak was varying between –4.24 V to –4.31 V and this variation was less frequent comparatively. The RMS fluctuation was found to vary between 2.96 to 3.03 V.

b) Long time stability

For this, the voltage signal after being converted to current is injected across a constant resistance network through I1 and I2 shown in Fig 5.1. Then the voltage is picked up through E1 and E2 of the ICG instrument. The demodulated output is taken at test point TP5 (Fig 3.6) for every 10 minutes and it was found to be very stable at

+2.365 V. Thus, it was concluded that the high frequency variation in the peak values of the sinusoid is well beyond the bandwidth of the impedance detector circuit.

5.2 Voltage-to-current converter

The performance of the unbalanced voltage-to-current converter was tested by injecting a sinusoid of constant frequency and amplitude. The frequency was kept at 92 kHz and the current generated by the converter was ≈ 3 mA with the input being at 2.96 V_{rms}. The load R_L between I1 and I2 (Fig 3.2) was varied and the current generated for various loads was calculated from the voltage drop across the resistance, and is given in Table 5.1 below. The output voltage was taken at I1 and I2 and the difference was used to calculate the I_{rms}.

Table 5.1 Loading characteristics of V/I converter in unbalanced mode

R_L (Ω)	218.9	149.5	100.4	56.4	47.1	39.0	22.2	15.1	10.1
I_{rms} (mA)	2.67	2.72	2.71	2.85	2.85	2.85	2.83	2.82	2.89

There was a 1 – 5 MHz interference on the output. For load resistance $R_L < 33$ Ω, making measurement on the output voltage (and hence the current) became difficult because of this interference. The cause of the interference was investigated. The two electrode leads were connected through shielded cables to reduce external RF pick-up. The shields were grounded to reduce electrostatic pick-up. It was found that the removal of grounding of I2 shield did not have an effect on the interference. However, removal of grounding of I1 shield removed the interference. Hence it was concluded that the interference was caused most likely due to low level high frequency oscillations in opamp U3 (Fig 3.2) because of the cable shield capacitance getting connected between the inverting terminal and ground. Hence it was decided to use ungrounded shields. A better solution would be to use buffers for driving the shields. The recordings for the Table 5.1 was done with the ungrounded shields.

The balanced current source was tested separately. In this case electrode lead I11 is high impedance point. It was observed that a grounded shield for this output caused high frequency oscillation similar to that in the unbalanced V/I converter. Hence it was

decided to use ungrounded shields. In further modified version, buffers for driving the shields may be used.

Balanced V/I converter was tested for different loads, and it was verified that voltage outputs at I11 and I22 were balanced with respect to ground with in 16 mV_{rms}. The load current for different loads was also measured and is given in the Table 5.2

Table 5.2 Loading characteristics of V/I converter in balanced mode

R_L (Ω)	218.9	149.5	100.4	56.4	47.1	39.0	22.2	15.1	10.1
I_{rms} (mA)	2.62	2.70	2.76	2.80	2.82	2.82	2.84	2.84	2.89

5.3 Instrumentation amplifier of ICG

The instrumentation amplifier was tested for its ability to pick up differential signal and to reject common mode signal. The response of the amplifier is shown in Fig 5.2. The graph shows the CM and DM gains of the amplifier at various frequencies.

For differential mode, the input was set at E_1 = 200 mV and E_2 = 0. The output was taken at test point TP4. The gain was found to be +19.6 dB at ≈ 100 kHz. For common mode, the input are E_1 = E_2 = 6 Vp-p. The gain was found to be –22.9 dB at 100 kHz. The CMRR at 100 kHz was found to be +42.5 dB. A plot of CMRR vs frequency is shown in Fig 5.3.

5.4 Demodulator

The test input, which is a 1 Hz sinusoid modulated at 1% depth by a carrier of 100 kHz frequency & 600 mVp-p magnitude is injected at TP4. The output taken at TP5 in Fig 3.6 was a perfect sinusoid of frequency 1 Hz and magnitude 17 mVp-p with an offset of 463.4 mV. This was repeated for various frequencies of the signal, modulation depth, and carrier magnitudes. The result was found to be satisfactory.

5.5 DC cancellation circuit

A sinusoid of frequency 2 Hz, and amplitude 120 mVp-p with an offset of +2 V DC was given as input to the drift cancellation circuit (Fig 3.6) at test point TP5. As the gain of the DC cancellation circuit is 10, the sinusoid with the DC offset will get saturated

at the output of the DC cancellation circuit. This is overcome by the correction provided by the microcontroller and low pass filter section of the circuit. The output of the circuit is shown in Fig 5.4. The correction period was found to be 10 ms. The frequency of the sinusoid at the input was varied and it was found that the performance of the DC cancellation circuit to be stable up to 10 Hz and the correction was provided effectively till an offset of 7 V.

Also the circuit was tested using the simulator that was designed to calibrate the ICG instrument. The simulator was put in the ICG mode. The current is injected into the simulator through I1 and I2 from the ICG instrument and the voltage from E1 and E2 is picked up from the simulator. The output $z(t)$ of the ICG instrument is shown in Fig 5.5. The switching frequency of the simulator in ICG mode was varied from 1 – 4 Hz and the output was noted to be a square wave with the same frequency. The amplitude was well maintained between –1 to –2.5 V after DC cancellation. There was a high frequency noise component riding over this square wave output. The frequency of this component was found to be between 4 – 5 MHz.

5.6 ECG amplifier

The instrumentation amplifier section of the ECG amplifier was tested for its ability to reject CM and DM signal. The response of the same is shown in Fig 5.6. The 3-dB upper cutoff frequency was 22 Hz and the pass band gain was 19.3 dB for an input of 205 mV sinusoid. The CMRR for various frequencies is shown in Fig 5.7.

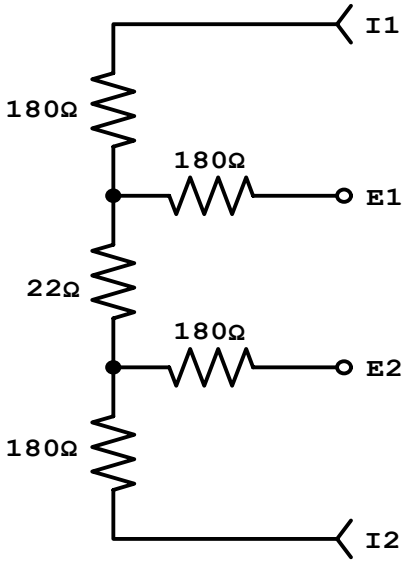

Fig 5.1 Resistive network used for testing the long term stability of oscillator

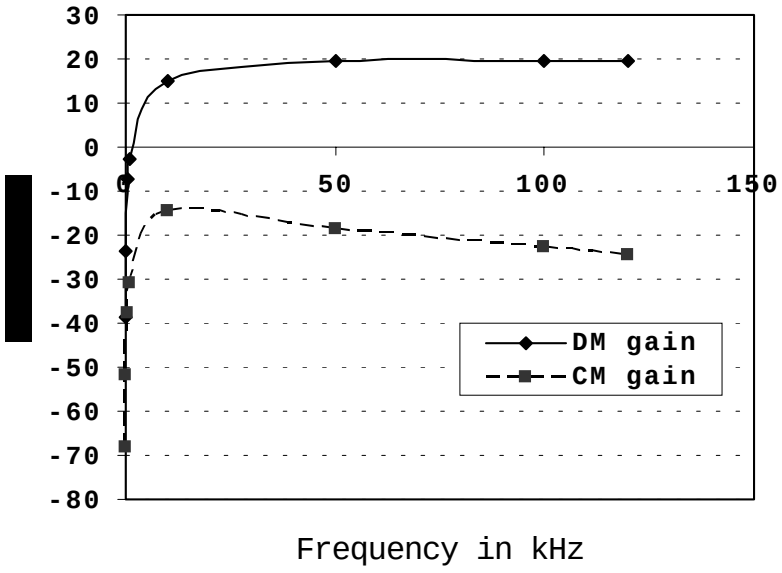

Fig 5.2 CM/DM vs frequency of ICG instrumentation amplifier

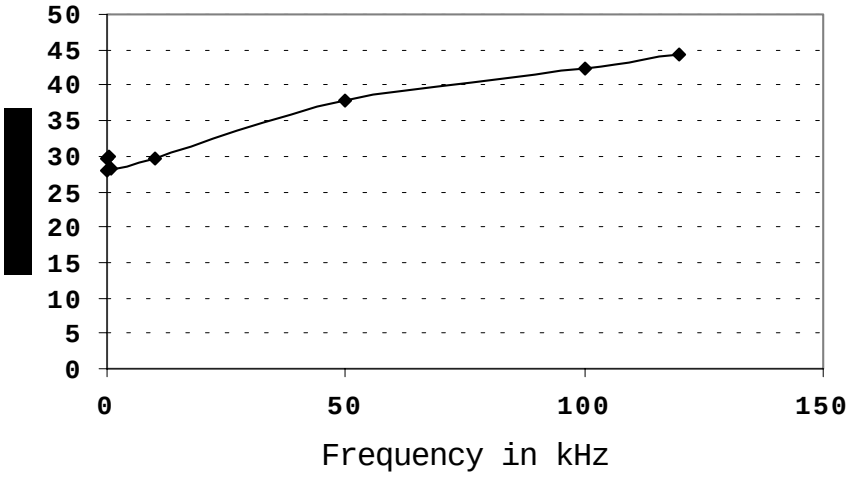

Fig 5.3 CMRR vs frequency of ICG instrumentation amplifier

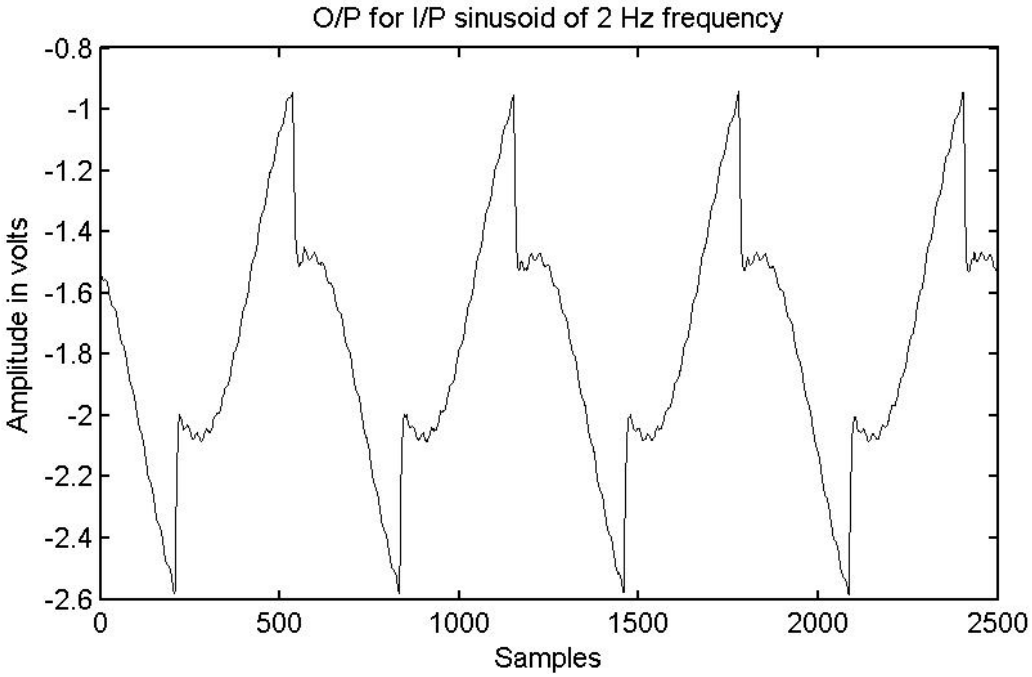

Fig 5.4 Test output of DC cancellation circuit with sinusoidal input

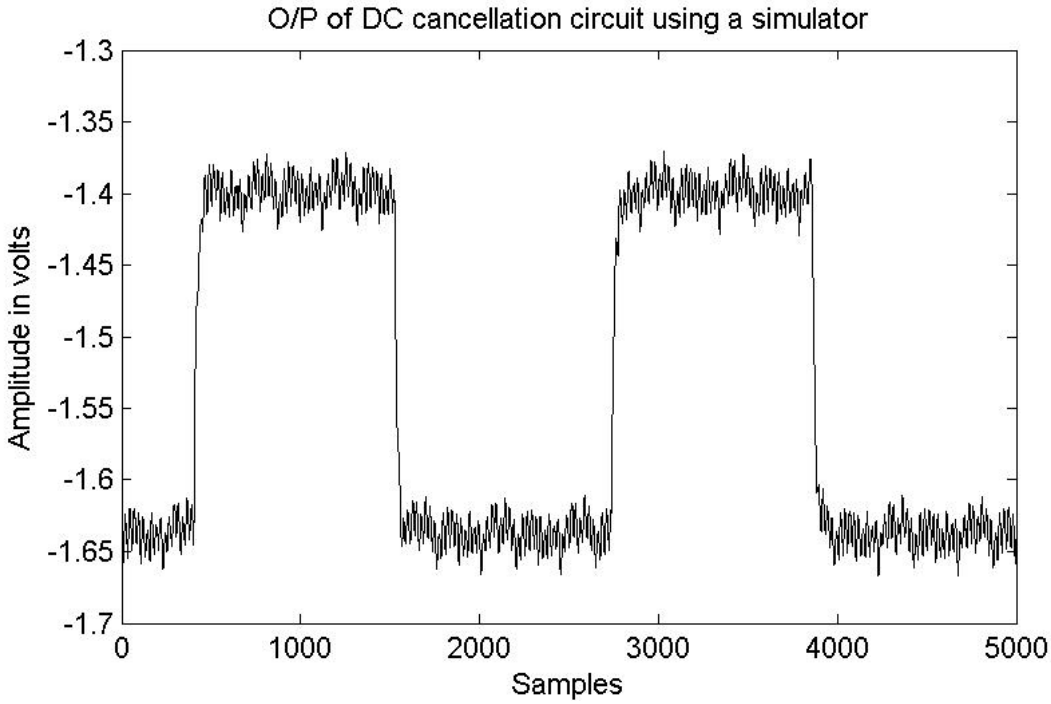

Fig 5.5 Output of DC cancellation circuit with simulator

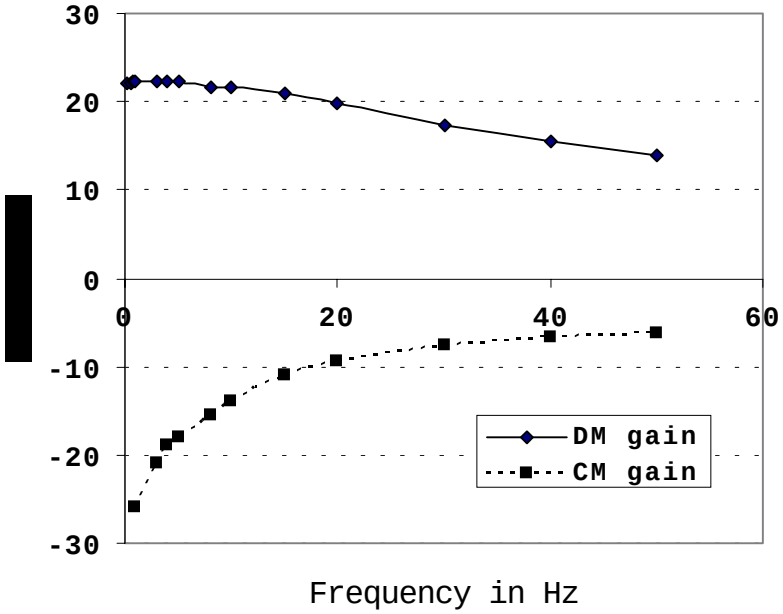

Fig 5.6 CM/DM vs frequency of ECG amplifier

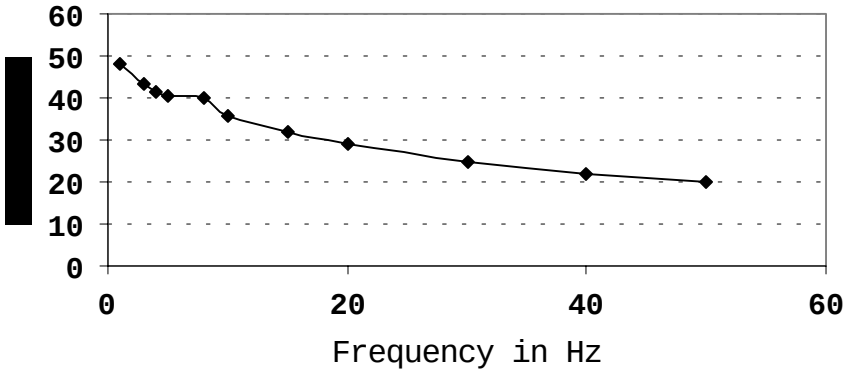

Fig 5.7 CMRR vs frequency of ECG amplifier

Chapter 6
TEST RESULTS OF IMPEDANCE CARDIOGRAPHY

The ICG recordings were done in two modes: (a) unbalanced current injection mode, and (b) balanced current injection mode. All the recordings were taken on healthy subjects both under normal and post exercise conditions that is during relaxation after exercise. In all the recordings, both the current injection and voltage pick-up electrodes were placed on the front side of the thoracic region. The recordings were done at room temperature and the electrodes used were suction cup electrodes.

6.1 Unbalanced current injection mode

The unbalanced current injection mode is selected using the jumper JM2 shown in Fig 3.1. The ICG signal recorded simultaneously along with the ECG and PCG signals from subject NSM are shown in Fig 6.1. These signals were directly acquired from the impedance cardiograph using the data acquisition unit (Appendix B) with sampling rate of 1 k samples/s. These signals were then digitally filtered using filters developed in SPI Lab by V. K. Pandey and described in Appendix C, to remove the noise and motion artifacts. The filtered waveform is shown in Fig 6.2. The various final outputs after digitally processing the signals shown in Fig 6.1 are $z(t)$, dz/dt, Z_o, ECG, and PCG. The subject was in supine position and the distance between the voltage pick-up electrodes was 83 mm.

The distance between the voltage pick-up and current injection electrodes was varied and various recordings were done. Also the recording done on subject VKP in unbalanced current mode is shown in Fig 6.5 and the processed output is shown in Fig 6.6. Here the distance between the voltage pick-up electrodes were at 45 mm.

6.2 Balanced current injection mode

The jumper JMP2 is properly configured to operate the ICG instrument in balanced current injection mode. The recording were done on the same two subjects with the distance between the voltage pick-up electrodes being same as that of the unbalanced current injection mode and the results were compared. The magnitude spectrum of the ICG signal acquired from both balanced and unbalanced current modes were studied and it was noted that the noise level in both was almost equal. Further in unbalanced mode harmonics of 34 Hz was observed. The recordings done in balanced current mode are shown in Fig 6.3, 6.4, 6.7, and 6.8.

A detailed recording of ICG signals with ECG and PCG was done in various positions for subject 'SP' and the corresponding signals are shown in Fig 6.9 – 6.14. The cardiac output was calculated from all these recordings and is tabulated below in Table 6.1.

Table 6.1 Cardiac outputs of various subjects under various conditions, assuming blood resistivity of 150 Ω-cm

Subject	Sex	Status	Position	L in mm	Z_o in Ω		Cardiac output in L/min	
					Unbal. mode	Bal. mode	Unbal. mode	Bal. mode
NSM	Male	Normal	Supine	83	49.30	47.55	1.3	1.7
			Sitting					
		Post exercise	Supine					
SP	Male	Normal	Supine	87	24.12	23.12	3.6	4.3
			Sitting	87	30.20	28.35	1.4	1.2
		Post exercise	Supine	87	25.01	23.82	9.3	9.0
VKP	Male	Normal	Supine	50	19.80	22.98	2.2	3.7
			Sitting					
		Post exercise	Supine					

6.3 Recording from normal subjects

Recordings were done from normal subjects with time history and the cardiac outputs were calculated and are tabulated below. The recordings were done in normal condition and post exercise relaxation condition. The blood pressure was taken at the starting of normal condition and again at the end of the recording in post exercise relaxation condition. The recordings were done in unbalanced current mode.

Table 6.2 Table showing the recorded output of the subject NSM before exercise in sitting position assuming blood resistivity of 150 Ω-cm (BP at the starting: 118/81)

Subject: NSM, Sex: Male, Height: 177 cm, Weight: 73 kg, Body temp: 97.5 °F, L = 100 mm			
Time	Beat rate/min	Z_o	Cardiac output (L/min)
5.25 pm	80	38.20	2.8
5.30	79	38.98	2.4
5.35	79	40.48	2.1
5.40	77	37.46	1.9
5.45	76	39.25	1.9
5.50	76	39.48	1.8
5.55	77	40.48	1.9
6.00	76	40.14	1.8
6.05	76	42.95	1.7
6.10	73	43.15	1.5

Table 6.3 Table showing the recorded output of the subject NSM after exercise in supine position assuming blood resistivity of 150 Ω-cm (BP at the end of exercise: 115/75)

Subject: NSM, Sex: Male, Height: 177 cm, Weight: 73 kg, Body temp: 97.5 °F, L = 100 mm			
Time	Beat rate/min	Z_o	Cardiac output (L/min)
6.30 pm	118	39.73	3.8
6.35	93	39.29	4.1
6.40	85	39.05	4.1
6.45	89	39.06	4.2
6.50	86	39.19	3.5
6.55	84	39.15	3.9
7.00	87	39.27	3.3
7.05	78	39.74	3.0
7.10	77	39.99	3.0
7.15	75	39.73	3.3

Table 6.4 Table showing the recorded output of the subject VKP before exercise in supine position assuming blood resistivity of 150 Ω-cm (BP at the starting: 114/76)

Subject: VKP, Sex: Male, Height: 170 cm, Weight: 56 kg, Body temp: 96.9 °F, L = 114 mm			
Time	Beat rate/min	Z_o	Cardiac output (L/min)
1.15 pm	62.6	20.58	19.2
1.20	67.8	21.10	19.8
1.25	64.4	20.46	19.2
1.30	65.7	20.52	19.4
1.35	61.7	20.58	16.5
1.40	63.0	20.38	16.1
1.45	60.0	20.75	33.3

1.50	58.4	20.04	15.9
1.55	60.2	20.25	16.6
2.00	58.0	20.44	10.4

Table 6.5 Table showing the recorded output of the subject VKP after exercise in supine position assuming blood resistivity of 150 Ω-cm (BP at the end of exercise: 109/84)

Subject: VKP, Sex: Male, Height: 170 cm, Weight: 56 kg, Body temp: 96.9 °F, L = 114 mm			
Time	Beat rate/min	Z_o	Cardiac output (L/min)
2.25 pm	78.5	21.84	26.9
2.30	71.3	21.76	24.3
2.35	68.4	21.83	23.7
2.40	65.4	21.75	24.5
2.45	61.9	21.67	19.1
2.50	65.8	21.30	20.8
2.55	64.1	20.90	23.1
3.00	62.0	20.68	21.8
3.05	66.6	20.59	12.6
3.10	68.5	21.04	23.6

Table 6.6 Table showing the recorded output of the subject PL before exercise in supine position assuming blood resistivity of 150 Ω-cm (BP at the starting: 112/78)

Subject: PL, Sex: Male, Height: 168 cm, Weight: 59 kg, Body temp: 97.1 °F			
Time	Beat rate/min	Z_o	Cardiac output (L/min)
3.45 pm	88.1	25.00	10.4
3.50	78.7	24.57	8.0
3.55	85.9	24.29	14.5

4.00	81.6	23.74	7.2
4.05	86.7	23.90	13.5
4.10	81.8	23.86	6.6
4.15	86.0	24.03	7.9
4.20	82.1	23.57	7.9
4.25	78.3	24.54	7.1
4.30	78.2	24.24	7.8

Table 6.7 Table showing the recorded output of the subject PL after exercise in supine position assuming blood resistivity of 150 Ω-cm (BP at the end of exercise: 102/66)

Subject: PL, Sex: Male, Height: 168 cm, Weight: 59 kg, Body temp: 97.1 °F			
Time	Beat rate/min	Z_o	Cardiac output (L/min)
4.40 pm	152.2	24.90	16.4
4.45	123.4	24.90	14.5
4.50	119.1	25.41	11.7
4.55	116.9	25.18	12.7
5.00	112.3	24.90	10.6
5.05	111.5	24.67	6.6
5.10	110.3	24.93	9.8
5.15	107.3	24.62	9.6
5.20	102.7	24.53	8.6
5.25	104.2	24.50	8.1

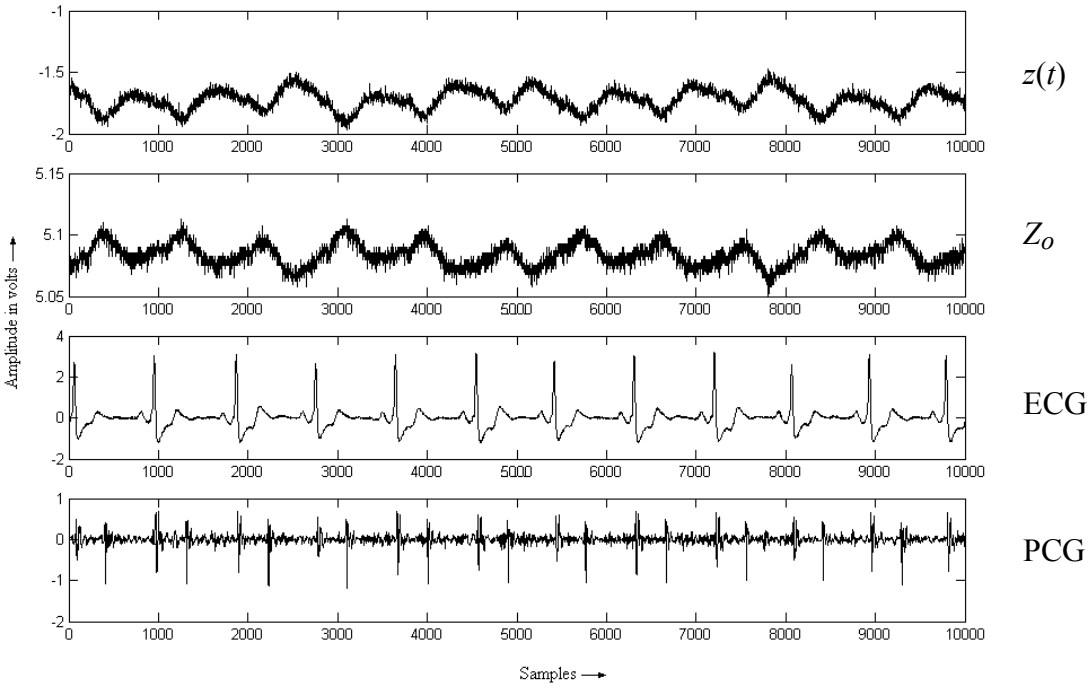

Fig 6.1 Signals recorded from subject 'NSM' with the ICG instrument with unbalanced current source (100 samples = 100 ms).

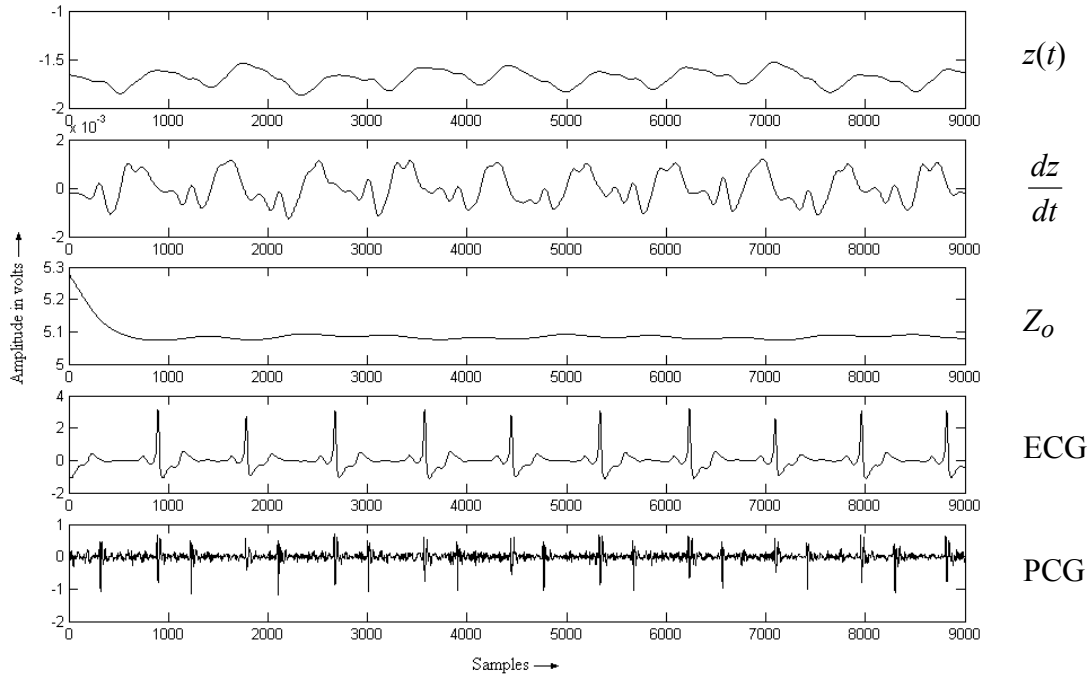

Fig 6.2 Processed output of signal in Fig 6.1 (100 samples = 100 ms).

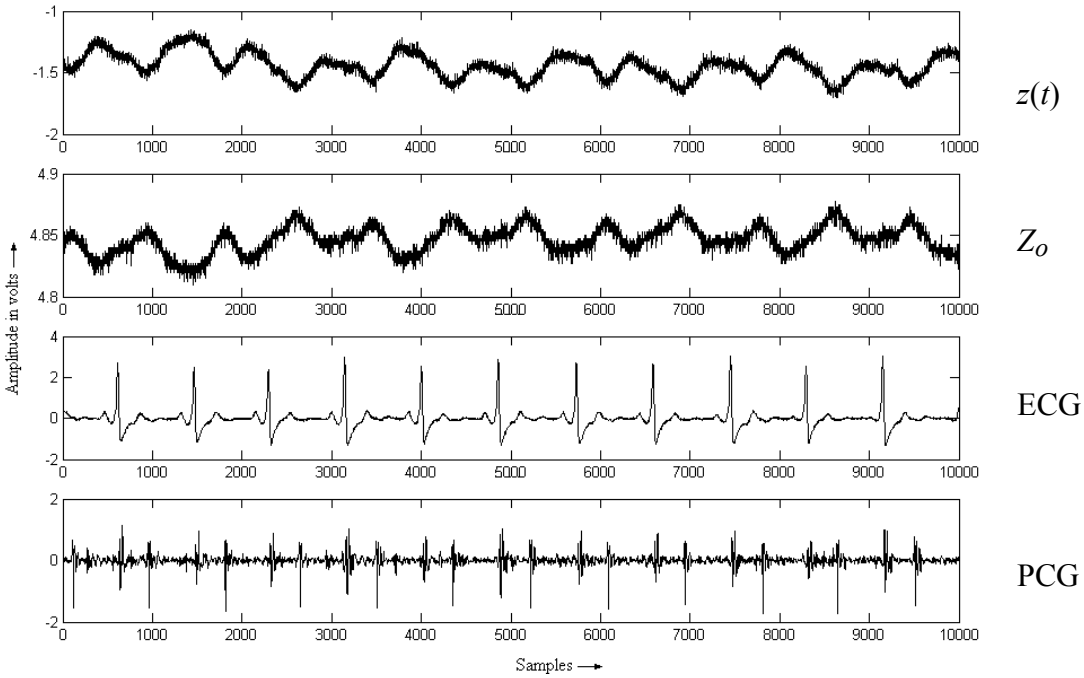

Fig 6.3 Signals recorded from subject 'NSM' with the ICG instrument with balanced current source (100 samples = 100 ms).

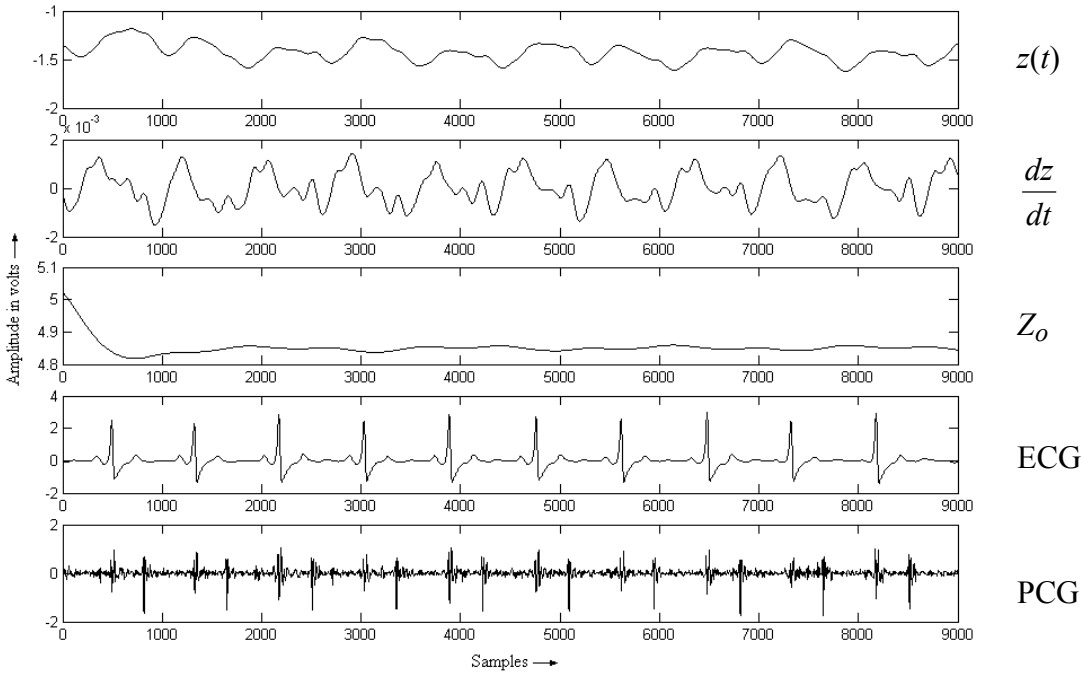

Fig 6.4 Processed output of signal in Fig 6.3 (100 samples = 100 ms).

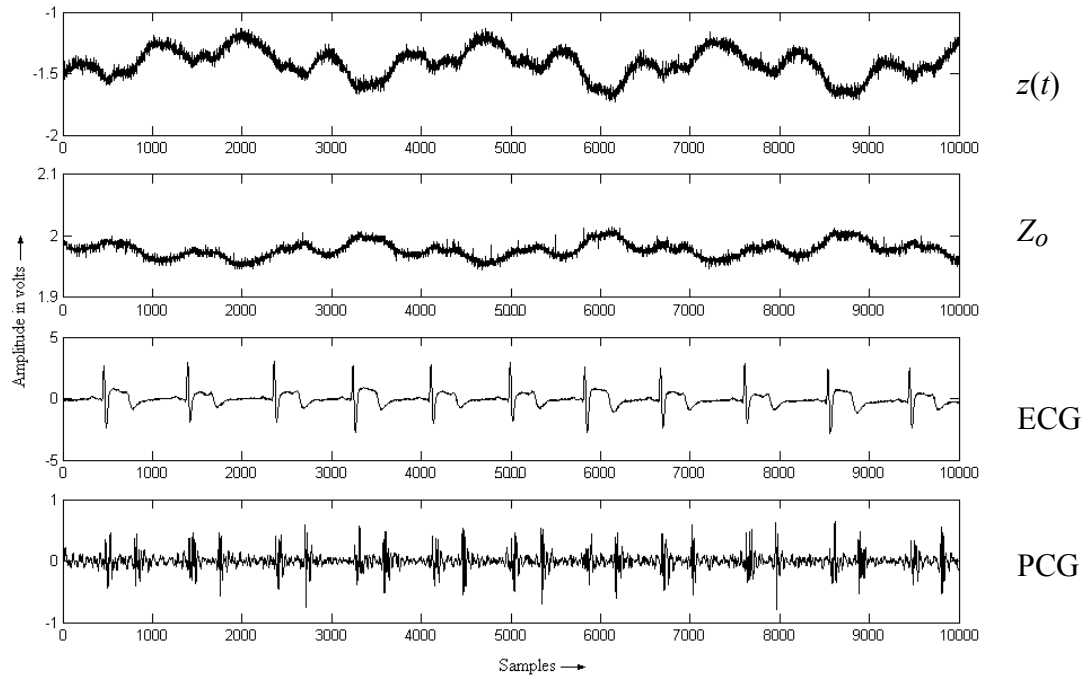

Fig 6.5 Signals recorded from subject 'VKP' with the ICG instrument with unbalanced current source (100 samples = 100 ms).

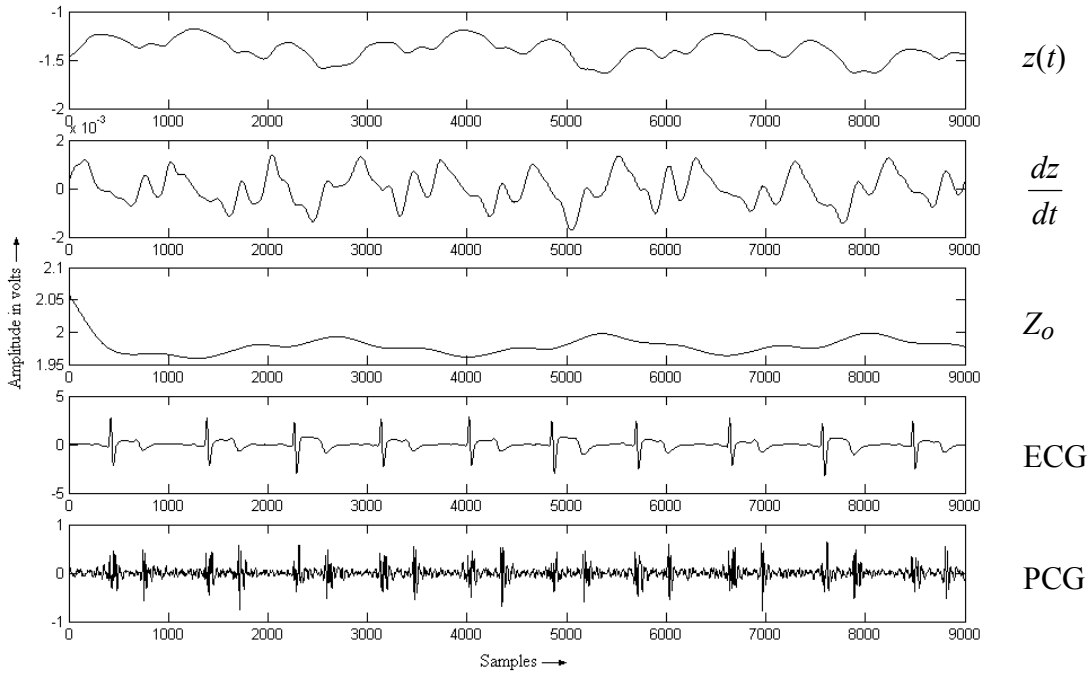

Fig 6.6 Processed output of signal in Fig 6.5 (100 samples = 100 ms).

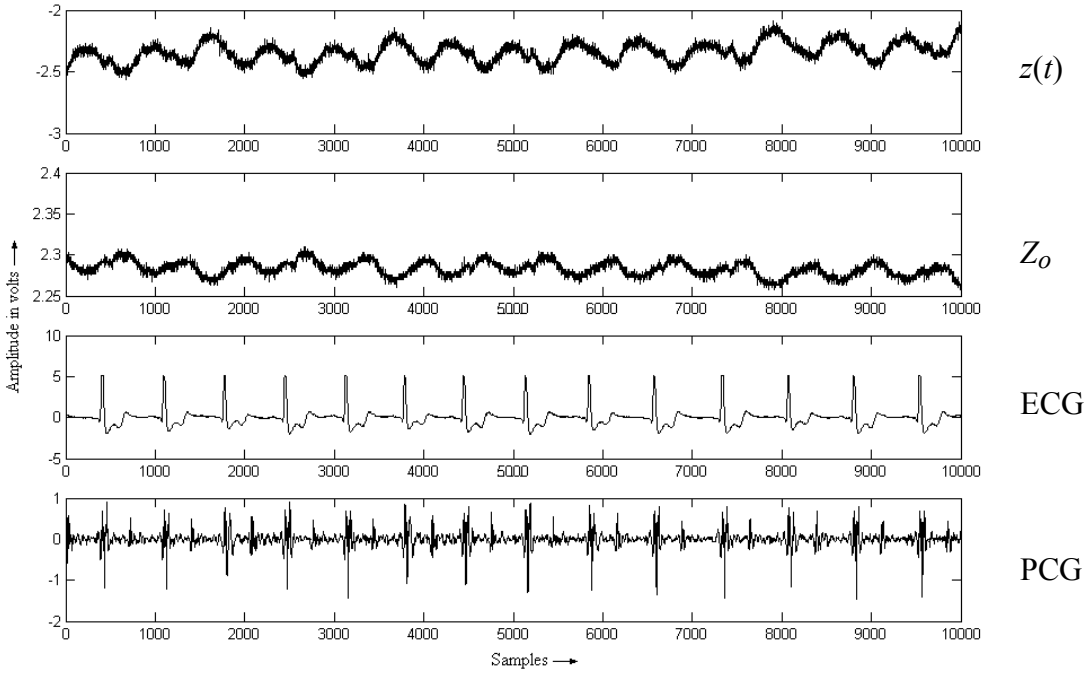

Fig 6.7 Signals recorded from subject 'VKP' with the ICG instrument with balanced current source (100 samples = 100 ms).

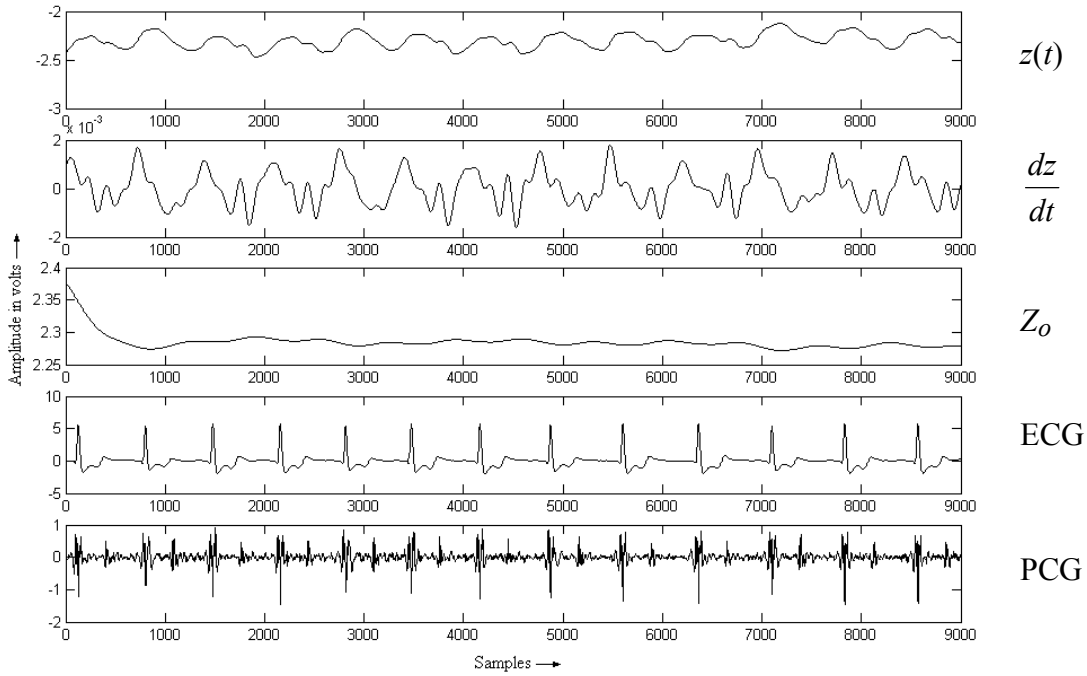

Fig 6.8 Processed output of signal in Fig 6.7 (100 samples = 100 ms).

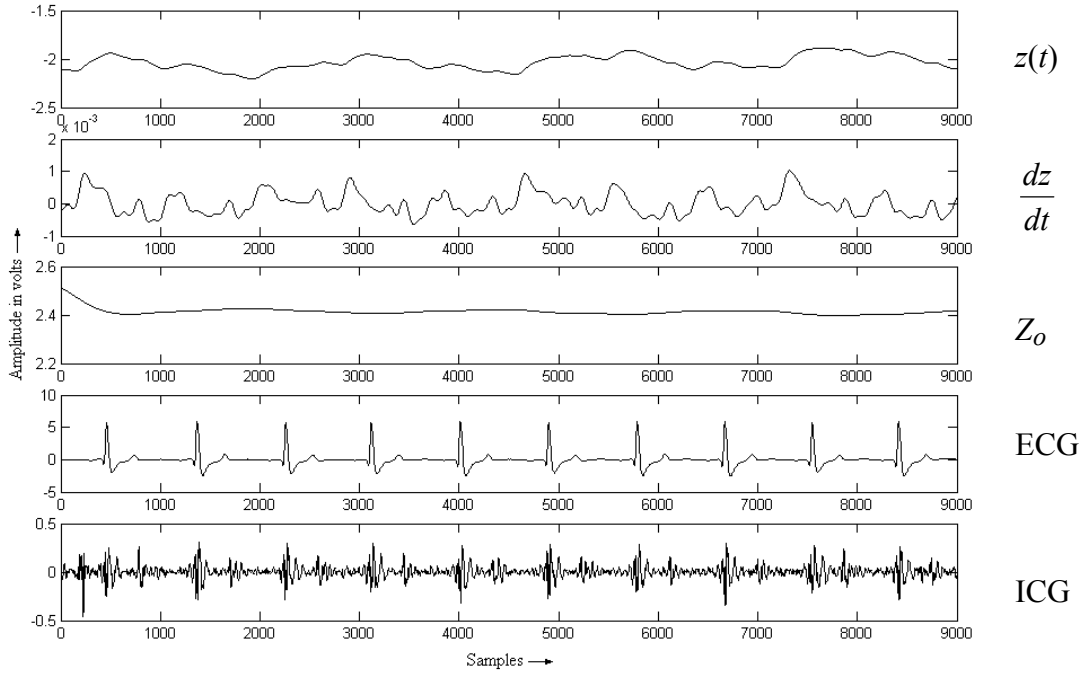

Fig 6.9 Signals recorded from subject 'SP' with the ICG instrument with unbalanced current source in supine position (100 samples = 100 ms).

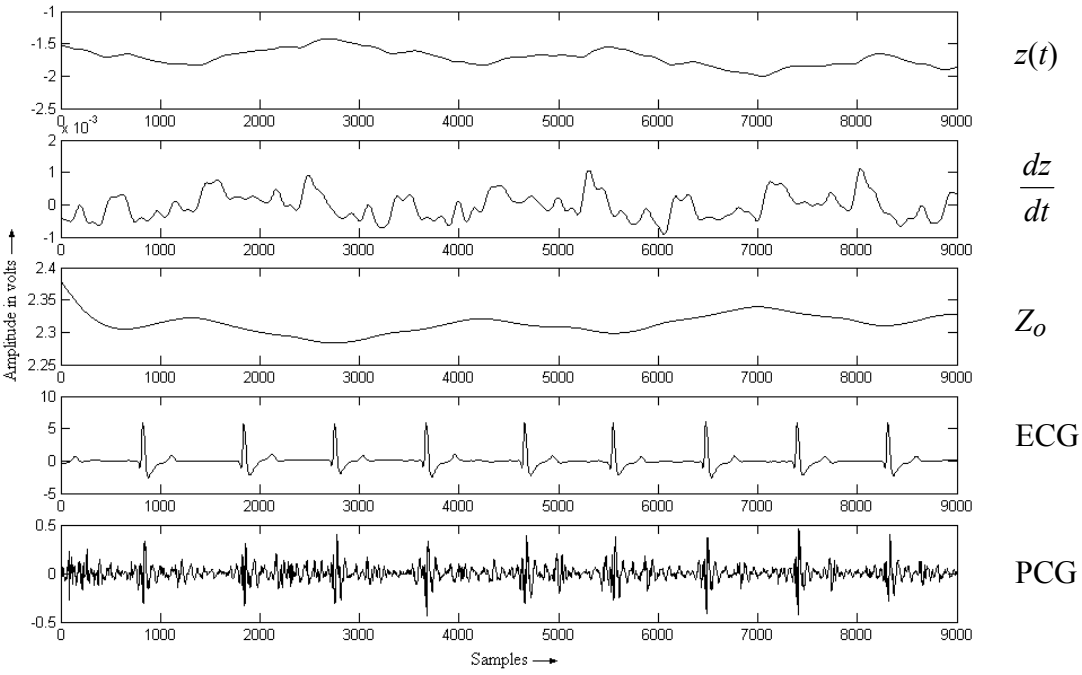

Fig 6.10 Signals recorded from subject 'SP' with the ICG instrument with balanced current source in supine position (100 samples = 100 ms).

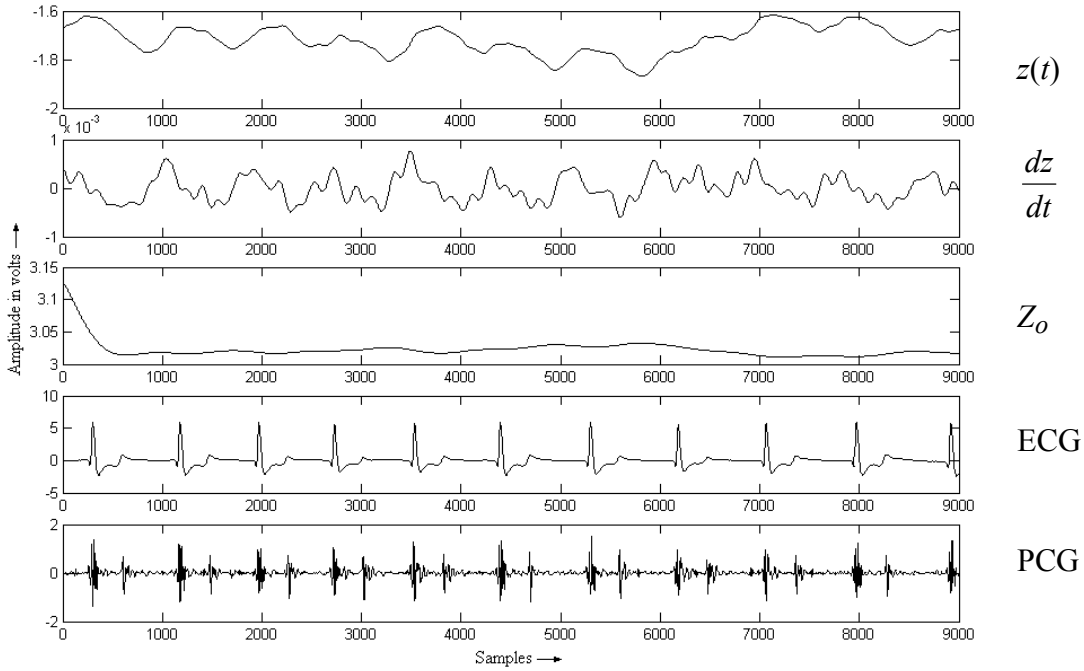

Fig 6.11 Signals recorded from subject 'SP' with the ICG instrument with unbalanced current source in sitting position (100 samples = 100 ms).

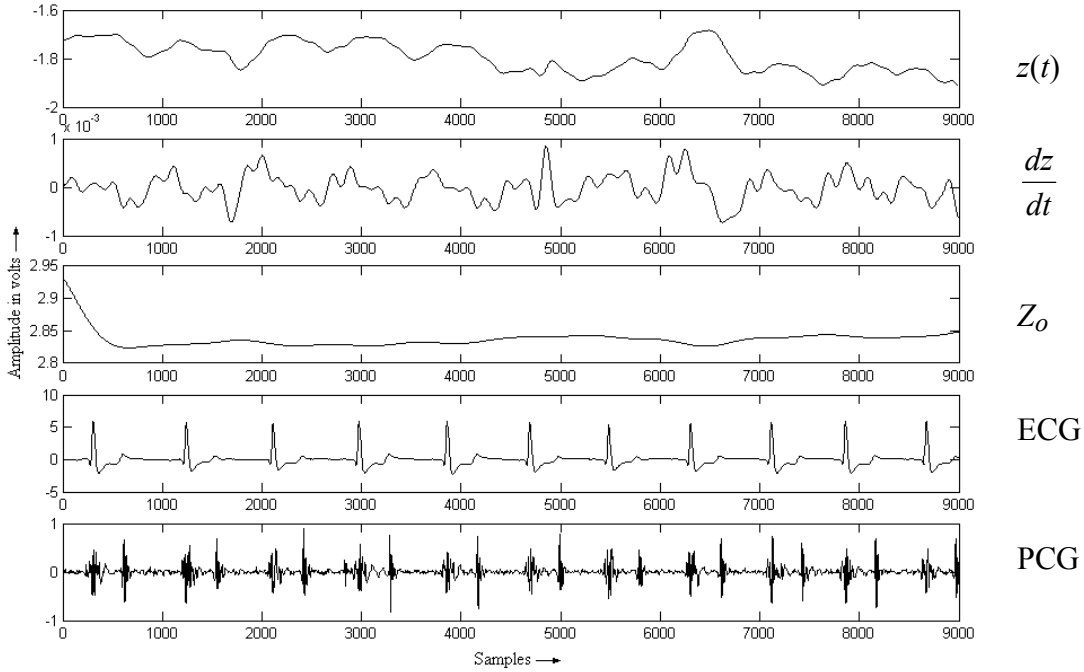

Fig 6.12 Signals recorded from subject 'SP' with the ICG instrument with balanced current source in sitting position (100 samples = 100 ms).

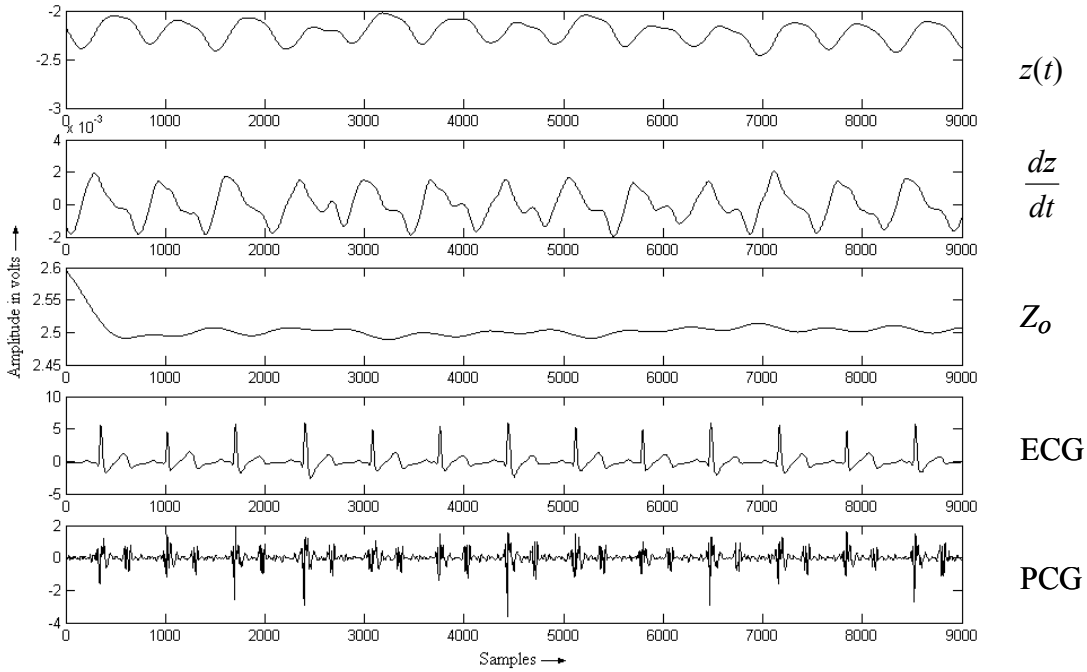

Fig 6.13 Signals recorded from subject 'SP' with the ICG instrument with unbalanced current source in supine position after exercise (100 samples = 100 ms).

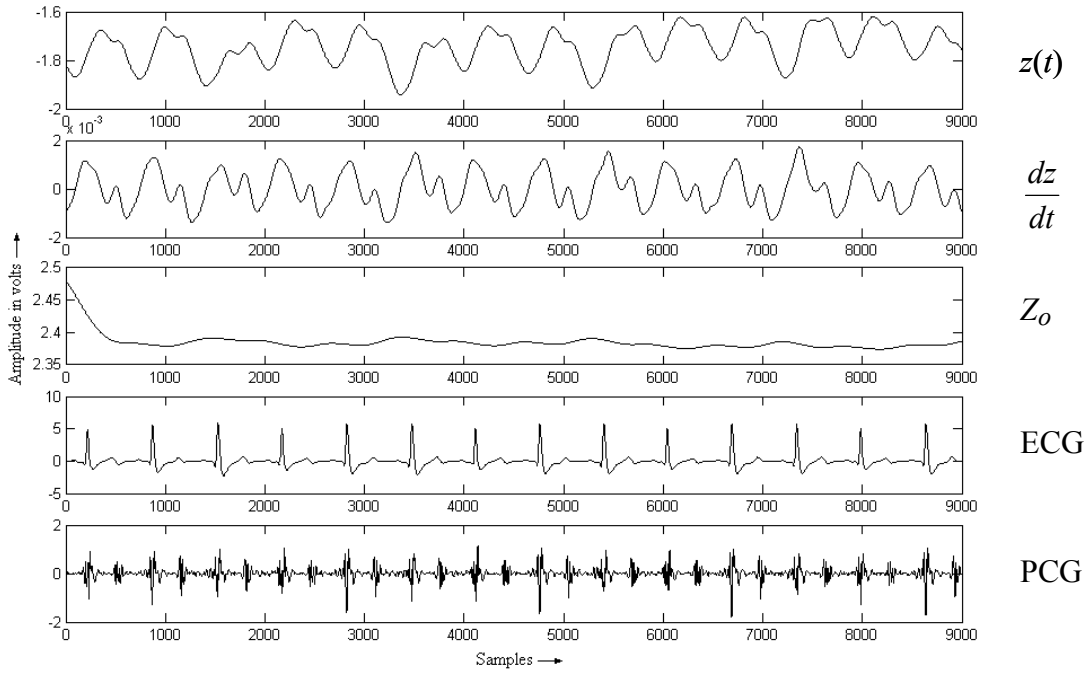

Fig 6.14 Signals recorded from subject 'SP' with the ICG instrument with balanced current source in supine position after exercise (100 samples = 100 ms).

Chapter 7
CONCLUSION

7.1 Summary of work done

The project objective was to develop a hardware for impedance cardiography, making use of the previous designs, and making appropriate modifications. The project was executed in three stages. In first stage the thoracic simulator was built and tested. In stage two, the PWM based DC cancellation circuit was built and the thoracic impedance simulator was redesigned for various basal impedances. Finally in third stage the impedance cardiograph instrument was built. The PCB was made, tested, and boxed.

Recordings were taken on various normal subjects and the results were compared with the reported ones. The results were found satisfactory. A transformerless balanced current source was used for current injection. No significant difference in the result by the two was observed. Further the magnitude spectrum of the ICG signal recorded using unbalanced and balanced current sources was studied and it was noted that the noise components in both were almost same

7.2 Suggestions for future work

The oscillator section has to be redesigned to get a good short-time amplitude stability. Buffered shielding should be done for the cables at high impedance points in order to avoid noise oscillation from being introduced into the injected current signal. The demodulator section has to be modified using ICs having higher slew rate. Further, a power pack should be developed so that the instrument can operate from a single battery. The instrument then onwards may be useable for clinical recordings.

Currently we have taken data recordings from 5 normal subjects. To validate the instrument, we need to build up a database consisting of normal subjects and patients with

cardiac disorders. We can further categorise the latter into groups based on smoking habits, occupation, physical activities etc.

Appendix A

LIST OF COMPONENTS

Impedance cardiograph

Component designator	Part description	Component specification	Approx. price/unit in Rs.
R1, R49, R51, R68, R69, R70, R72, R89, R90	Resistor	1 MΩ, 1/4 Watt	0.20
R0, R2, R3, R7, R63, R65, R84, R86, R94	Resistor	1 kΩ, 1/4 Watt	0.20
R4, R5, R29, R33, R36, R62, R83	Resistor	15 kΩ, 1/4 Watt	0.20
R10, R11, R15, R18, R22–R26, R37, R43, R44, R50, R52, R56, R57, R71, R73, R77, R78, R91, R92, R96, R97, R99	Resistor	10 kΩ, 1/4 Watt	0.20
R8, R95	Resistor	2.2 kΩ, 1/4 Watt	0.20
R12, R13, R16, R19, R27, R28, R40, R45, R60, R81	Resistor	33 kΩ, 1/4 Watt	0.20
R53, R54, R55, R74, R75, R76	Resistor	39 kΩ, 1/4 Watt	0.20
R42, R93	Resistor	3.3 kΩ, 1/4 Watt	0.20
R20, R21, R39	Resistor	100 kΩ, 1/4 Watt	0.20
R30, R31, R32, R34a, R34b, R46	Resistor	22 kΩ, 1/4 Watt	0.20
R14, R17	Resistor	1.5 kΩ, 1/4 Watt	0.20
R98	Resistor	4.7 kΩ, 1/4 Watt	0.20
R9	Resistor	680 Ω, 1/4 Watt	0.20
R35	Resistor	120 kΩ, 1/4 Watt	0.20
R58, R59, R61, R79, R80, R82, R101	Resistor	82 kΩ, 1/4 Watt	0.20
R48, R100	Resistor	8.2 kΩ, 1/4 Watt	0.20
R47	Resistor	3.9 kΩ, 1/4 Watt	0.20
R41	Resistor	5.6 kΩ, 1/4 Watt	0.20
R67, R88	Resistor	3.3 MΩ, 1/4 Watt	0.20
R66, R87	Resistor	220 kΩ, 1/4 Watt	0.20
R64, R85	Resistor	12 kΩ, 1/4 Watt	0.20
R6, R38	Potentiometer	10 kΩ, Cermet	3.00
R102	Potentiometer	100 kΩ, Cermet	3.00
C1	Ceramic capacitor	22 nF	0.40

C2, C3, C13, C14	Ceramic capacitor	100 pF	0.40
C18, C20, C32, C33, C41, C42	Ceramic capacitor	47 nF	0.40
C37, C46	Ceramic capacitor	2.2 nF	0.40
C27, C28, C48, C51	Ceramic capacitor	22 pF	0.40
C77	Electrolytic capacitor	2.2 µF	1.00
C25, C26	Electrolytic capacitor	10 µF	1.00
C4–C6, C11, C12, C15–C17, C19, C21, C22, C29, C38, C47, C49, C50, C52, C55–C76, C78–C80	SMD capacitor 1206	0.1 µF	1.00
C7–C10, C23, C24, C30, C31, C34–C36, C39, C40, C43–C45, C53, C54	Ceramic capacitor	0.1 µF	0.80
D1, D2, D3, D4, D5, D6, D7, D8	Diode	IN4148	1.00
Z1, Z2	Zener	3V3	2.00
LED1, LED2	LED		1.50
TP1–TP5, JM1–JM3	Test pins		0.50
I1, I2, I11, I22, E1, E2, z(t), Zo, Vcp, ECG1, ECG2	RCA connectors		4.00
Ext I/P	2-Pin male connector		1.50
T1	FET	BFW10	27.00
U1–U3, U6–U10, U16–U19	Opamp	LF356	18.00
U4–U5	Comparator	LM311	7.00
U11, U13–U15	Opamp	TL084	10.00
U12	Microcontroller	89c2051	42.00
PCB	Double sided epoxy		600.00
		Total Cost	1090.00

Thoracic impedance simulator

Component designator	Part description	Component specification	Approx. price/unit in Rs.
R1, R2, R6, R13, R14, R25	Resistor	100 kΩ, 1/4 Watt	0.20
R3, R4, R10	Resistor	47 kΩ, 1/4 Watt	0.20
R5, R7	Resistor	10 kΩ, 1/4 Watt	0.20

R9	Resistor	1 MΩ, 1/4 Watt	0.20
R8	Resistor	15 kΩ, 1/4 Watt	0.20
R11, R12	Resistor	33 kΩ, 1/4 Watt	0.20
R15, R16, R24	Resistor	2.2 kΩ, 1/4 Watt	0.20
R17, R18	Resistor	100 Ω, 1/4 Watt	0.20
R19, R20	Resistor	820 Ω, 1/4 Watt	0.20
R21, R22	Resistor	680 Ω, 1/4 Watt	0.20
R26, R27, R28, R29	Resistor	220 Ω, 1/4 Watt	0.20
R23	Resistor	33 Ω, 1/4 Watt	0.20
P1, P2, P3	Potentiometer	100 kΩ, Wire wound	8.00
C1	Electrolytic capacitor	47 µF	1.00
C2–C5	Ceramic capacitor	0.1 µF	0.40
C6, C7, C8	Electrolytic capacitor	10 µF	1.00
D1, D2	Diode	IN4007	1.00
S1, S2	Switch	SPDT	8.00
S3, S4	Slide switch		10.00
U1, U2	IC	TL084	10.00
U3, U4, U5	IC	CD4066	9.00
		Total Cost	870.00

Appendix B
DATA ACQUISITION UNIT

The data acquisition unit that was used for acquisition of ICG signals was USBDAQ-9100-MS, manufactured by Adlink Technology (Taiwan). This unit has its own enclosure and can be interfaced to the PC using USB (universal serial bus).It has 16 single-ended or 8 differential 12-bit A/D input channel and 2 D/A outputs. Its important features are given below

- Simultaneous sampling of 4 analog channels
- On board 4 K samples FIFO buffer
- Up to 100 ksamples/s continuous A/D sampling
- Programmable input range
- 8 isolated digital input and 8 isolated digital output
- Two general purpose timer/counter (8254) with programmable interface

The unit has been tested and software for signal acquisition has been developed in our lab by Vinod Kumar Pandey. The graphical user interface (GUI) of the program is developed in Visual Basic. The acquisition program uses A/D driver routines for acquisition of the signals. The data are sampled at specified sampling rate and for specified number of samples. The specifications of the program are

- Sampling frequency: 1 Hz to 100 kHz
- Buffer size: 100 samples to 4 k samples
- Channels: 8 (maximum 4 channel simultaneously)
- Output format: binary/text

Appendix C
DIGITAL FILTERING OF ICG

Impedance cardiogram $z(t)$, basal impedance Z_o, ECG, and PCG signals were simultaneously acquired using USB based data acquisition card. Acquired signals have strong noise contamination. These signals are digitally filtered to remove noise. As shown in Fig C.1, this filtering scheme has been (jointly) worked out in our lab by Vinod Kumar Pandey and described in his Ph.D progress seminar report.

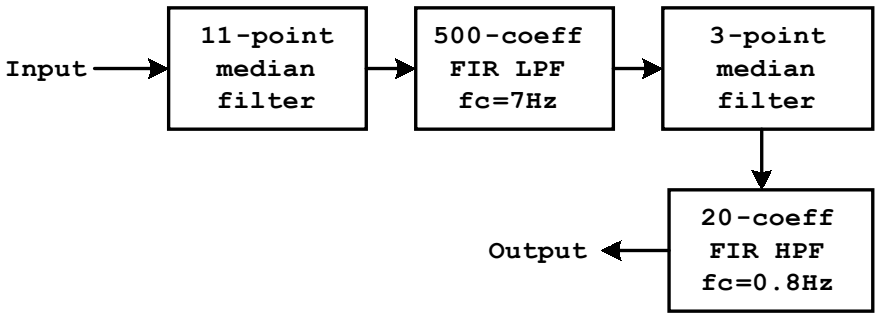

Fig C.1 Filtering of ICG signal

Filtered $z(t)$ signal is differentiated, using 2-point differentiator to get *dz/dt* waveform.

Acquired Z_o is superimposed on slow variation of impedance cardiogram signal with large DC value. For getting the mean value of Z_o, the acquired Z_o was passed through Butterworth low pass filter of order 2 and cutoff frequency 0.8 Hz.

The *dz/dt* waveform have uncertain fluctuations and it is difficult to get B and X points from the same. Sometimes *dz/dt* waveform contains motion artifacts, not fully attenuated by the filter. To remove remaining motion artifacts and for better detection of B and X point, ensemble averaging technique is used.

ECG R-point is used as a fudicial mark for averaging *dz/dt* waveform. Acquired ECG is processed as shown in Fig C.2 to locate the R-point. ECG is first passed through 10^{th} order Butterworth low pass filter with cutoff of 40 Hz and 6^{th} order Butterworth high pass filter with cutoff of 9 Hz. After this band pass filtering, ECG signal is differentiated using 8-point differentiator, averaged and squared. For averaging, 64-points moving

window with 50% decimation was used. The R-point location is then detected by comparing the peaks of filtered ECG signal with an adaptive threshold.

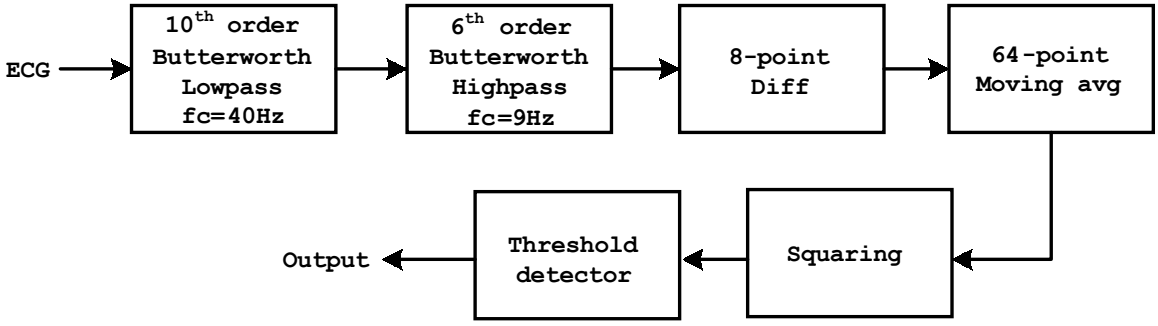

Fig C.2 Process of filtering for R-point detection of ECG

Appendix D

PCB LAYOUT

Impedance cardiograph:

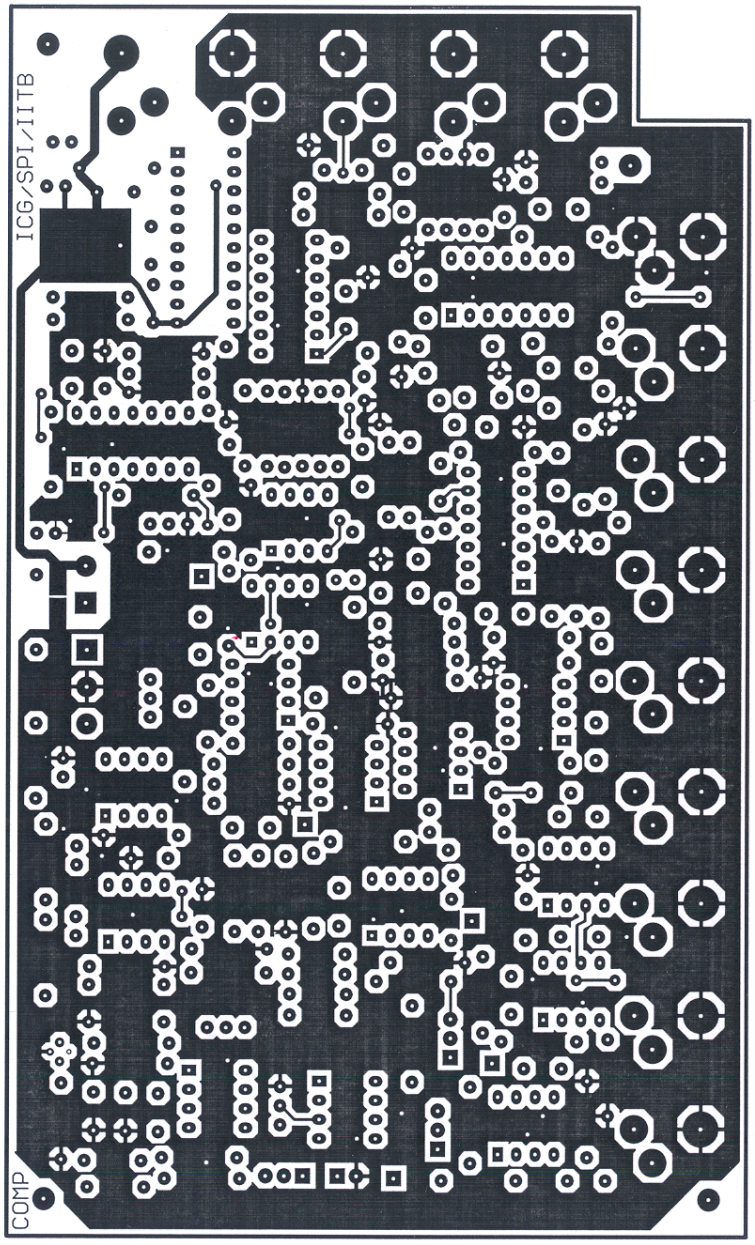

Fig D.1 Component side of impedance cardiograph PCB

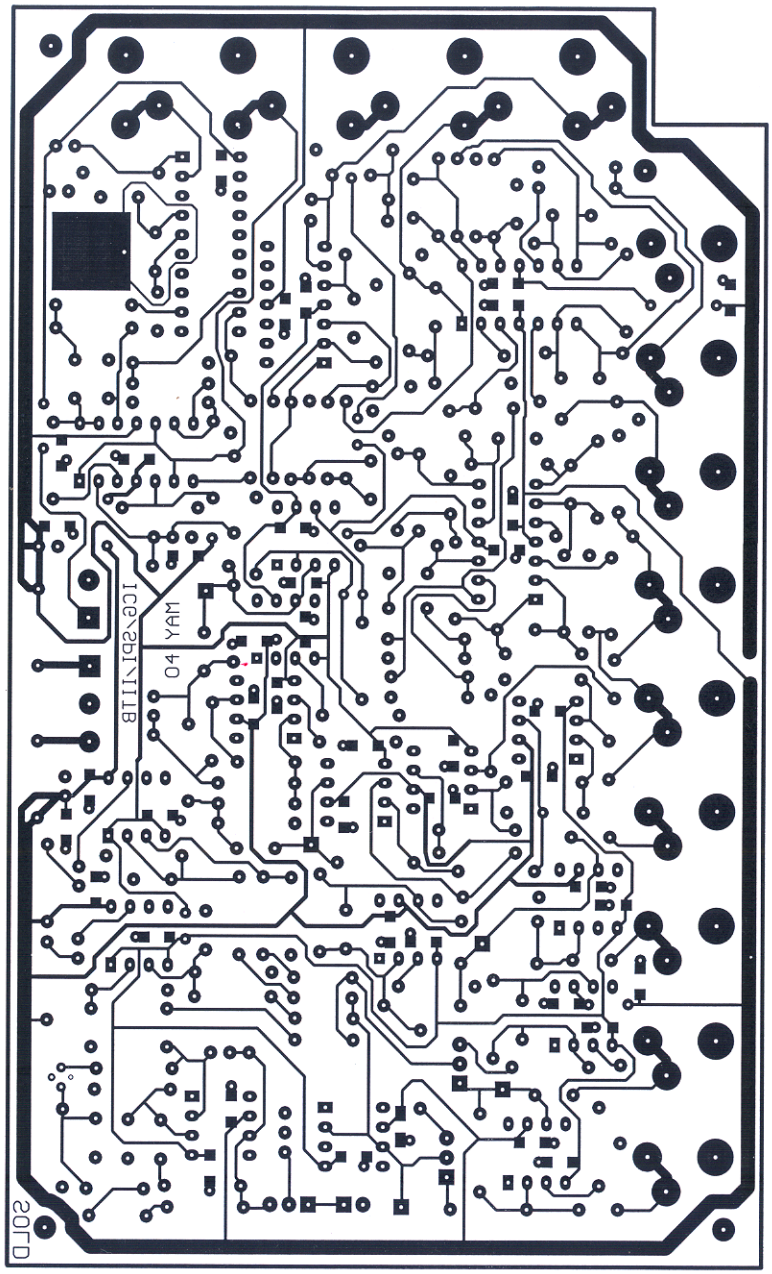

Fig D.2 Solder side of impedance cardiograph PCB

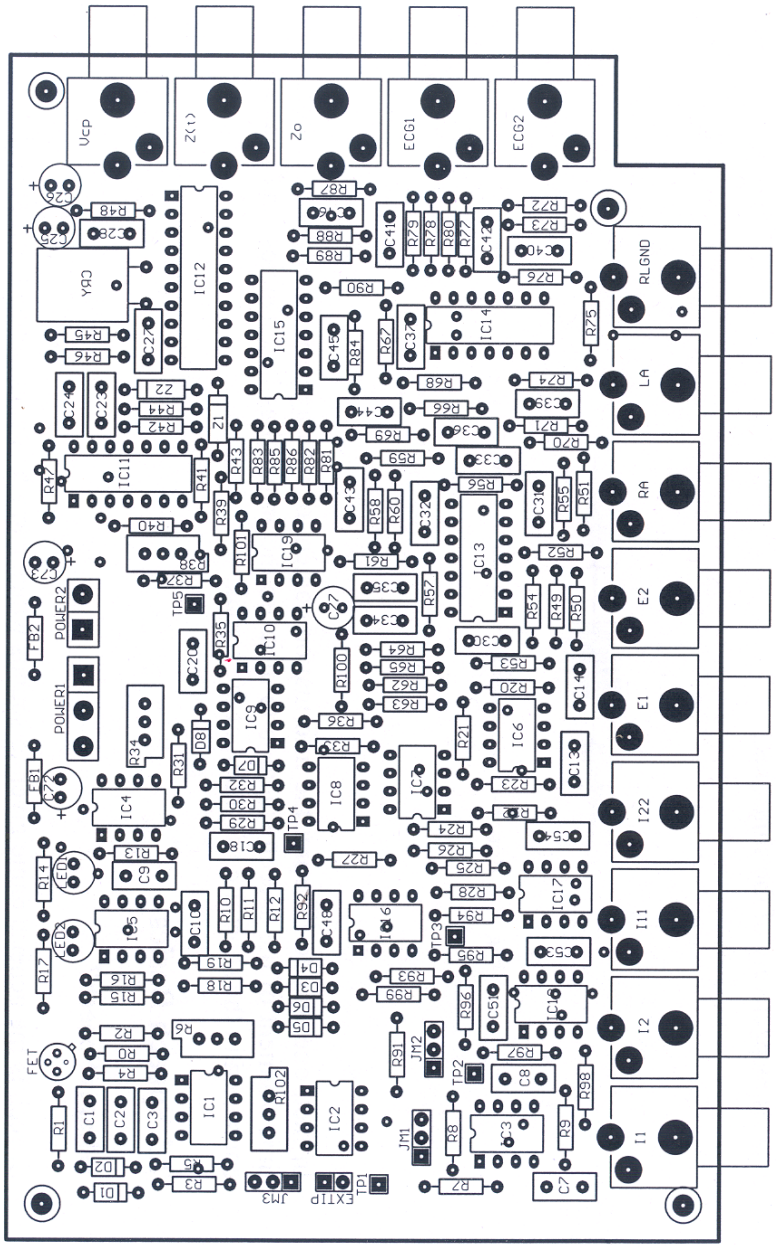

Fig D.3 Component layout of impedance cardiograph PCB

Thoracic impedance simulator

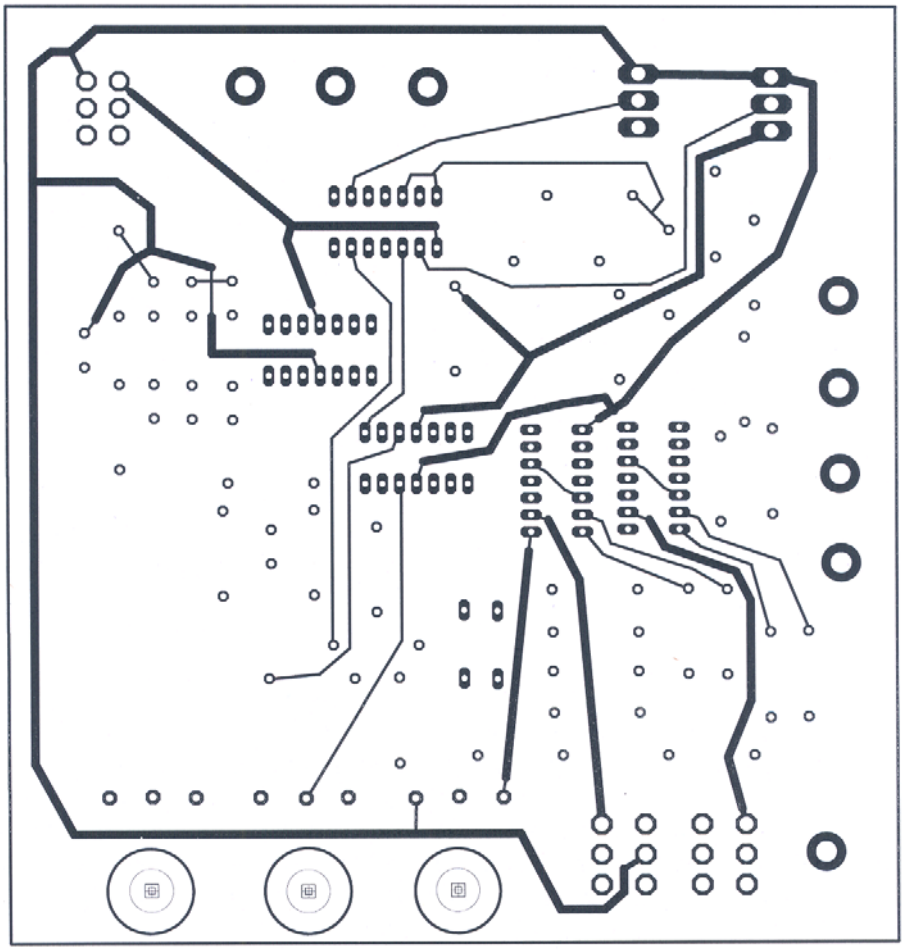

Fig D.4 Component side layout of simulator PCB

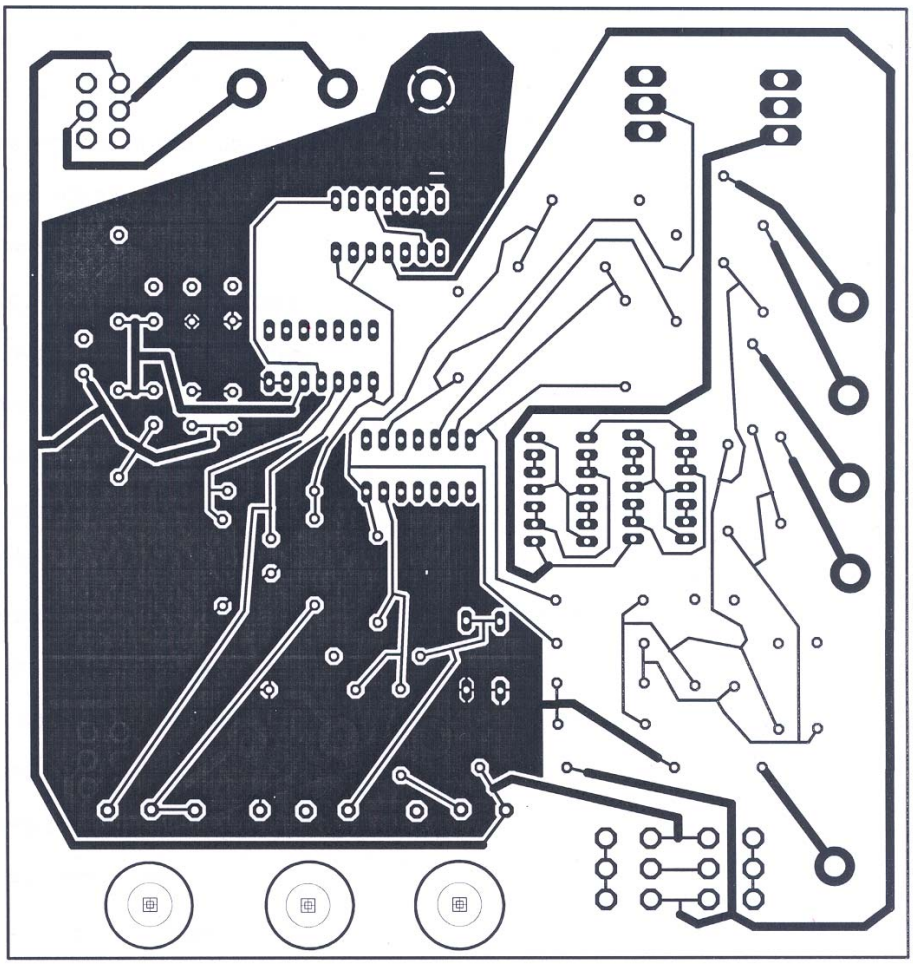

Fig D.5 Solder side layout of simulator PCB

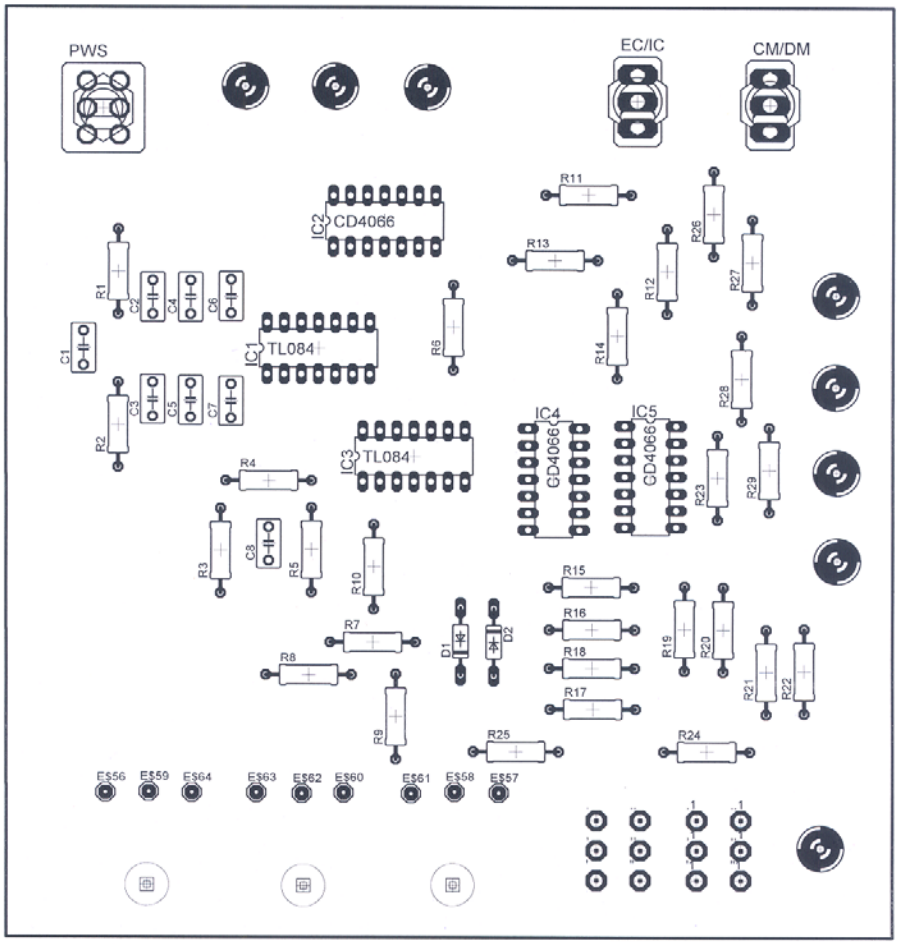

Fig D.6 Component placement layout of simulator PCB

Appendix E
ENCLOSURE LAYOUT

Impedance cardiograph

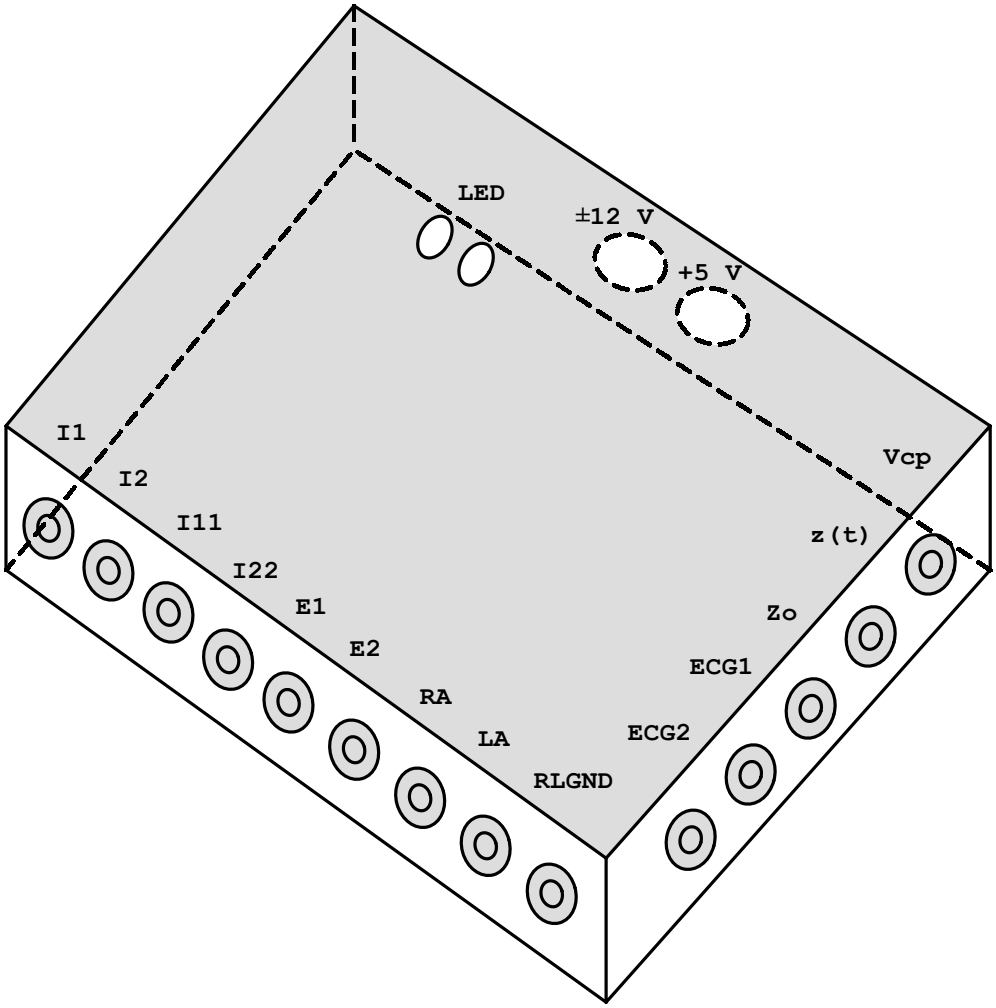

Fig E.1 Enclosure for impedance cardiograph

Thoracic impedance simulator

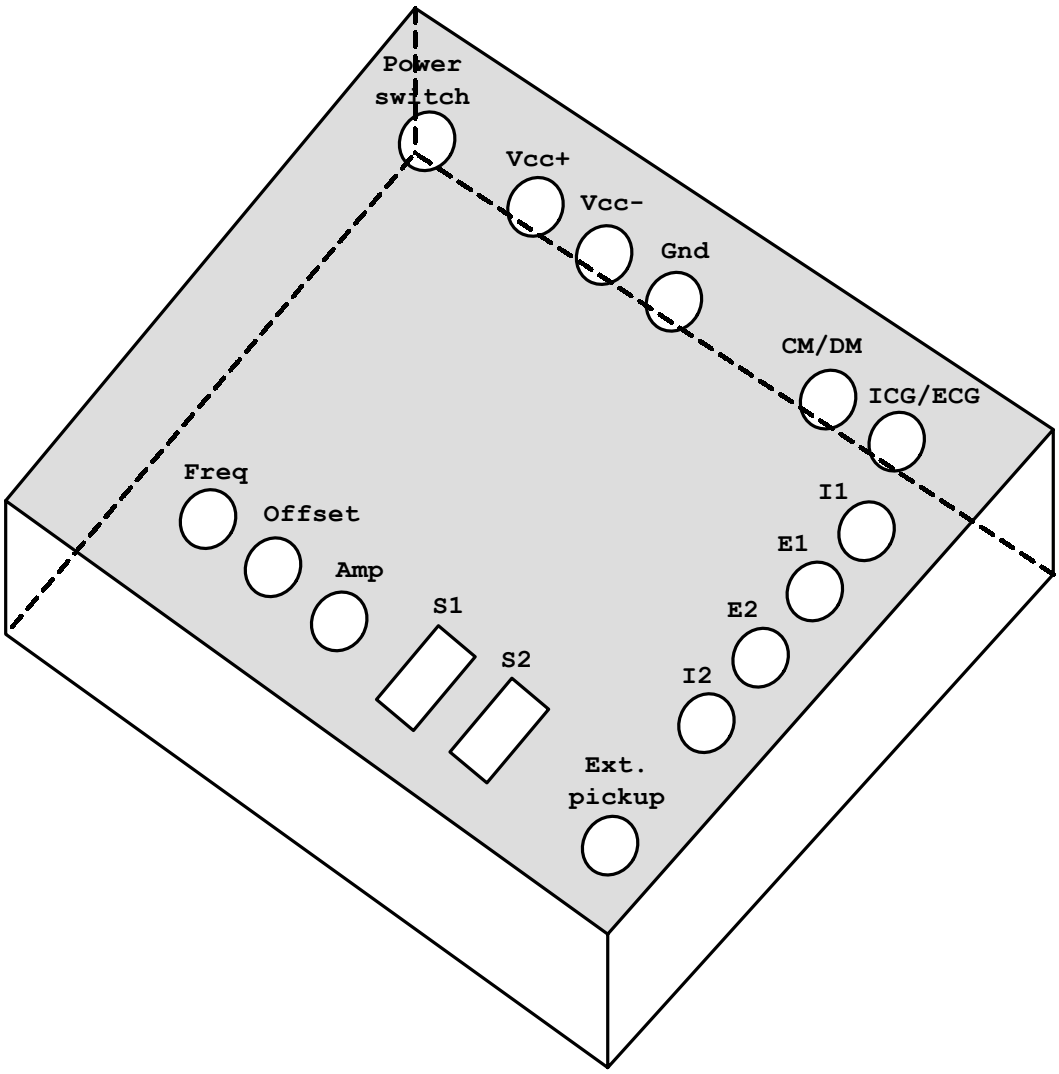

Fig E.2 Enclosure for thoracic impedance simulator

Appendix F
POWER REQUIREMENT

Impedance cardiograph

1. Excitation circuit and ICG extraction circuit

Power supply	-	±12 V regulated DC source
Current	-	100 mA, each.

2. Microcontroller

Power supply	-	+5 V regulated DC source
Current	-	50 mA

Thoracic impedance simulator

Power supply	-	± 4.5 V to ± 12 V dc.
Current	-	10 mA approx.

REFERENCES

[1] L. A. Geddes, and L. E. Baker, *Principles of Applied Biomedical Instrumentation*, 3rd ed. New York: Wiley, 1989.

[2] B. B. Sramek, "Thoracic electrical bioimpedance: basic principles and physiologic relationship," *Noninvasive Cardiology* (Irvine, USA). vol. 3(2), pp. 83–88, 1994.

[3] R. P. Patterson, "Fundamentals of impedance cardiography," *IEEE Eng, Med. Biol. Mag.,* vol. 8, No. 1, pp. 35–38, Mar. 1989.

[4] T. Palko, F. Bialokoz, and J. Weglarz, "Multifrequency device for measurement of the complex electrical bio-impedance – design and application," *in Proc. 14th Int. Conf. IEEE-EMBS & Biomedical Eng. Society of India*, New Delhi, pp. 1.45–1.46, Feb. 1995.

[5] L. E. Baker, "Principles of the impedance technique," *IEEE Eng. Med. Bio. Mag*., pp. 11–15, Mar. 1989.

[6] M. Qu., Y. Zhang, J. G. Webster, and W. J. Tompkins, "Motion artifact from spot and band electrodes during impedance cardiography," *IEEE Trans. Biomed. Eng.,* vol. BME-33, No. 11, pp. 1029–1036, Nov. 1986.

[7] Y. Zhang, M. Qu, J. G. Webster, W. J. Tompkins, B. A. Ward, and D. R. Bassett Jr, "Cardiac output monitoring by impedance cardiography during treadmill exercise," *IEEE Trans. Biomed. Eng*., vol. BME-33, No. 11, pp. 1037–1042, Nov. 1986.

[8] H. J. Burgess, P. D. Penev, R. Schneider, and E. V. Cauter, "Estimating cardiac autonomic activity during sleep: impedance cardiography, spectral analysis, and poincare plots," *Int. Fed. of Clin. Neurophysiol*., vol. 115, pp. 19–28, 2004.

[9] L. Wang, and R. Patterson, "Multiple sources of the impedance cardiogarm based on 3-D finite difference human thorax models," *IEEE Trans. Biomed. Eng*., vol. 42, No. 2, pp. 141–147, Feb. 1995.

[10] D. M. Linton, and D. Gilon, "Advances in noninvasive cardiac output monitoring," *Annals of Cardiac Anaesthesia*, vol. 5, pp. 141–148, 2002.

[11] W. G. Kubicek, F. J. Kottke, M. U. Ramos, R. P. Patterson, D. A. Witsoe, J. W. Labree, W. Remple, T. E. Layman, H. Schoening, and J. T. Garamela, "The Minnesota impedance cardiograph – theory and applications," *Biomed. Eng*., vol. 9, pp. 410–416, Sep. 1974.

[12] L. Wang and R. Patterson, "Contributions of heart movement and blood volume change to impedance cardiography calculated by human thorax models," *in Proc. 15th Ann. Int. Conf. IEEE-EMBS*, pp. 808–809, 1993.

[13] A. P. DeMarzo, R. M. Lang, R. Priemer, and C. E. Korcarz, "Computer method of predicting the reliability of impedance cardiogarphy stroke volume measurements," *Comp. in Cardiol*., pp. 497–500, 1995.

[14] B. H. Brown, D. C. Barber, A. H. Morice, and A. D. Leathard, "Cardiac and respiratory related electrical impedance changes in the human thorax," *IEEE Trans. Biomed. Eng*., vol. 41, No. 8, pp. 729–734, Aug. 1994.

[15] E. Raaijmakers, T. J. Faes, H. G. Goovaerts, P. M. J. M. de Vries, and R. M. Heethaar, "The inaccuracy of Kubicek's one-cylinder model in thoracic impedance cardiography," *IEEE Trans. Biomed Eng*., vol. 44, No. 1, pp. 70–76, Jan. 1997.

[16] A. K. Deshpande, G. D. Jindal, P. M. Jagasia, K. V. S. Murali, P. A. Bharadwaj, K. I. Tahilkar, and G. B. Parulkar, "Impedance plethysmography of thoracic region: impedance cardiography," *Journal of post graduate medicine* (KEM Mumbai, India), vol. 36, No. 4, pp. 207–212, 1990.

[17] M. Ingle and P. C. Pandey, "Cardiac output monitoring with an impedance cardiograph," *in Proc. 14th Int. Conf. IEEE-EMBS & Biomedical Eng. Society of India*, New Delhi, India. Feb. 1995.

[18] S. M. Joshi and P. C. Pandey, "An impedance cardiograph," *in Proc. Second BIOMEDEA Symp.*, (IIT Bombay, India), pp. 23–25, Feb. 1994.

[19] S. M. Joshi and P. C. Pandey, "A cardiac output monitor using impedance plethysmography," *in Proc. Int. Conf. Recent Adv. in Biomed. Eng*., (Osmania Univ. Hyderabad, India), Jan. 1994.

[20] R. P. Patterson, "Sources of the thoracic cardiogenic electrical impedance signal as determined by a model," *IEE, Med. & Biol. Eng. & Comput*., vol. 23, pp. 411–417, Sep 1985.

[21] B. Kuriakose, "An impedance cardiograph," M.Tech. Dissertation, Supervisor: P. C. Pandey, BME Group, IIT Bombay, 2000.

[22] S. M. Joshi, "A cardiac output monitor," B.Tech. Project report, Supervisor: P. C. Pandey, EE Dept., IIT Bombay, 1993.

[23] K. S. Patwardhan, "An impedance cardiograph for stress testing," M.Tech. Dissertation, Supervisor: P. C. Pandey, EE Dept., IIT Bombay, 1997.

[24] A. C. Guyton, *Textbook of Medical Physiology,* 7th ed. Philadelphia, Pen: Saunders, 1986.

[25] J. G. Webster, *Medical Instrumentation-Application and Design*, 3rd ed., New Delhi: John Wiley, 1998.

[26] J. Malmivuo and R. Plonsey, *Bioelectromagnetism*, 2nd ed., New York: Oxford Univ. Press, 1995.

[27] Y. Wang, D. R. Haynor, and Y. Kim, "A finite-element study of the effect of electrode position on the measured impedance change in impedance cardiography," *IEEE Trans. Biomed. Eng*., vol. 48, No. 12, pp. 1390–1401, Dec. 2001.

[28] D. A. Robert, "Recent biomedical applications of four-electrode impedance measuring techniques," *Instrument Society of America, Biomedical Science Instrumentation*, vol. 3, pp. 309–325, 1987.

[29] E. Raaijmakers, J. T. Marcus, H. G. Goovaerts, P. M. J. M. de Vries, J. C. Faes, and R. M. Heethaar, "The influence of pulsative flow on blood resistivity in impedance cardiography," *in Proc. 18th Ann. Int. Conf. IEEE-EMBS*, Amsterdam. pp. 1957–1958, 1996.

[30] F. R. Dungan, *Op Amps & Linear Integrated Circuits for Technicians*, 2nd ed. Albany, New York: Delmar, 1992.

[31] J. M. Fiore, *Op Amps and Linear Integrated Circuits*, Albany, New York: Delmar, 2001.

[32] H. G. Goovaerts, T. J. C. Faes, E. Raaijmakers, R. M. Heethaar, "An electrically isolated balanced wideband current source: basic considerations and design," *Medical & Biological Eng. & Computing,* vol. 36 (5), pp. 598–603, Sep. 1998

[33] S. M. Joshi and P. C. Pandey, "Drift cancellation circuit," *in Proc. Second BIOMEDEA Symp.*, (IIT Bombay, India), pp. 57–58, Feb. 1994.

[34] Cardiothoracic surgery, Keck School of Medicine of University of Southern California, http://www.cts.usc.edu/graphics/heart-crosssection1.jpg, down loaded on 17th July 2003.

[35] J. P. Doohan, "Biological Sciences, Santa Barbara city college, Sanata Barbara, California" http://www.biosbcc.net/doohan/sample/images/heart/0283circulation.jpg, down loaded on 17th July 2003.